Published in final edited form as:

Immunity. 2021 January 12; 54(1): 84–98.e5. doi:10.1016/j.immuni.2020.10.022.

Competition for active TGFβ cytokine allows for selective retention of antigen-specific tissue resident memory T cells in the epidermal niche

Toshiro Hirai[1,2,14,*], **Yi Yang**[1,2,3,4], **Yukari Zenke**[1,2,5], **Haiyue Li**[1,2,6], **Virendra K. Chaudhri**[7], **Jacinto S. De La Cruz Diaz**[1,2], **Paul Yifan Zhou**[1,2], **Breanna Anh-Thu Nguyen**[1,2], **Laurent Bartholin**[8], **Creg J. Workman**[2,9], **David W. Griggs**[10], **Dario A. A. Vignali**[2,9,11], **Harinder Singh**[7], **David Masopust**[12], **Daniel H. Kaplan**[1,2,13,*]

[1]Department of Dermatology, University of Pittsburgh, Pittsburgh, PA 15261

[2]Department of Immunology, University of Pittsburgh, Pittsburgh, PA 15261

[3]Department of Dermatology, Xiangya Hospital, Central South University, Changsha, China

[4]The Third Xiangya Hospital, Central South University, Changsha, China

[5]Department of Dermatology, St. Luke's International Hospital, Tokyo, Japan

[6]School of Medicine, Tsinghua University, No. 1 Tsinghua Yuan, Haidian District, Beijing 100084, China

[7]Center for Systems Immunology and the Department of Immunology, University of Pittsburgh, Pittsburgh, PA, USA.

[8]«TGF-β & Pancreatic Cancer » lab, Centre de Recherche en Cancérologie de Lyon (CRCL), Centre Léon Bérard, INSERM 1052, CNRS 5286, Université de Lyon, Université Claude Bernard Lyon 1, Lyon, France

[9]Tumor Microenvironment Center, UPMC Hillman Cancer Center, Pittsburgh PA 15232

[10]Department of Molecular Microbiology and Immunology, Saint Louis University, MO 63104

[11]Cancer Immunology and Immunotherapy Program, UPMC Hillman Cancer Center, Pittsburgh PA 15232

[12]Department of Microbiology and Immunology, Center for Immunology, University of Minnesota, Minneapolis, MN 55455

[*]Corresponding authors: t-hirai@biken.osaka-u.ac.jp; Dankaplan@pitt.edu.

Author Contributions

T.H. and D.H.K. designed and interpreted experiments; T.H., Y.Y., Y.Z., H.L., J.S.D., P.Y.Z., and B.A.N. performed experiments; L.B., C.J.W., and D.A.A.V. contributed a critical reagents; V.K.C. and H.S. conducted the bioinformatics analysis.; D.M. and D.G. provided technical and conceptual assistance; T.H. and D.H.K. wrote the manuscript and all authors edited it.

Competing interests

D.G. is a consultant and equity holder of Indalo Therapeutics which provided compound CWHM-12. All other authors state no conflict of interest.

[13]Lead contact

[14]Current address: BIKEN Innovative Vaccine Research Alliance Laboratories, Research Institute for Microbial Diseases, Osaka University, Osaka, Japan

Summary

Following antigen-driven expansion in lymph node, transforming growth factor-β (TGFβ) is required for differentiation of skin-recruited $CD8^+$ T cell effectors into epidermal resident memory T cells (Trm) and their epidermal persistence. We found that the source of TGFβ supporting Trm cells was autocrine. In addition, antigen-specific Trm cells that encountered cognate antigen in the skin, and bystander Trm cells that did not, both displayed long-term persistence in the epidermis under steady-state conditions. However, when the active-TGFβ was limited or when new T cell clones were recruited into the epidermis, antigen-specific Trm cells were more efficiently retained than bystander Trm cells. Genetically enforced TGFβR signaling allowed bystander Trm cells to persist in the epidermis as efficiently as antigen-specific Trm cells in both contexts. Thus, competition between T cells for active TGFβ represents an unappreciated selective pressure that promotes the accumulation and persistence of antigen-specific Trm cells in the epidermal niche.

eTOC blurb

Epidermal residence of $CD8^+$ memory T cells requires TGFβ, but the source of this cytokine and the relevance of this requirement are unclear. Hirai *et al.* reveal that intraclonal competition for transactivation of autocrine TGFβ preferentially enriches for antigen-specific T cells at the skin barrier.

Graphical Abstract

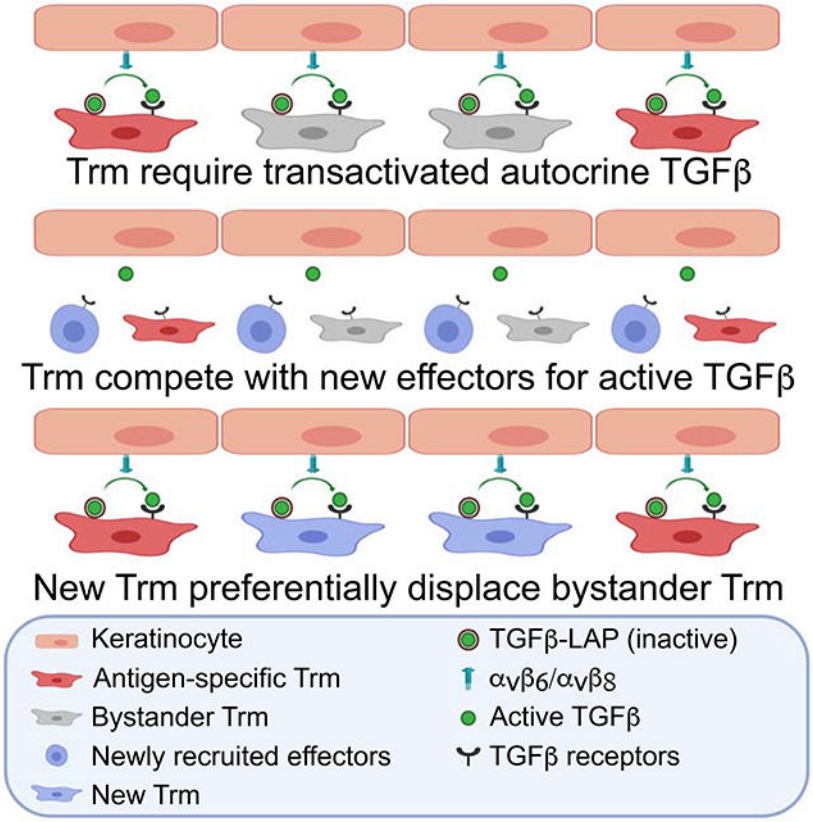

INTRODUCTION

Tissue resident $CD8^+$ memory T cells (Trm) are a highly abundant, noncirculating subset of memory T cells that provide efficient peripheral immune surveillance (Masopust and Soerens, 2019). In the skin, cutaneous infection with vaccinia virus (VV) or herpes simplex virus is well described to result in the development of large numbers of Trm cells that preferentially reside in the epidermis (Gebhardt et al., 2011; Hirai et al., 2020; Jiang et al., 2012). In these models, viral-derived antigen is initially brought to skin-draining lymph nodes by dendritic cells or through lymph which drives the expansion of $CD8^+$ T cell effectors (Allan et al., 2003; Bedoui et al., 2009; Liu et al., 2006; Reynoso et al., 2019). These effectors are then recruited into the sites of infected skin where they re-encounter antigen and some differentiate into long-lived Trm cells. In certain tissues such as the lung, re-encounter with cognate antigen in peripheral tissue is required for Trm cells differentiation (Lee et al., 2011; McMaster et al., 2018). In flank skin, however, a secondary encounter with cognate antigen is not required. For example, epicutaneous application of the sensitizing hapten 1-Fluoro-2,4-dinitrobenzene (DNFB) efficiently “pulls” non-antigen-specific, bystander effector cells expanded by viral infection or *in vitro* activation into the skin where they then differentiate into Trm cells (Mackay et al., 2012). Antigen-specific and bystander DNFB-pulled Trm cells appear phenotypically similar (Park et al., 2018) though potential functional differences have not been well explored.

The cytokine transforming growth factor β (TGFβ) is required for the development of Trm cells in many tissues such as skin, gut, and lung (Casey et al., 2012; Mackay et al., 2013; Sheridan et al., 2014; Wakim et al., 2015). TGFβ appears to be required at multiple steps in Trm cell development. Naïve steady-state $CD8^+$ T cells require TGFβ in order to maintain their potential to differentiate into Trm cells (Mani et al., 2019). In the skin, $CD8^+$ T cell effectors recruited by viral infection depend on TGFβ to differentiate into Trm cells (Mackay et al., 2013; Mackay et al., 2015). Exposure of $CD8^+$ T cells to TGFβ *in vitro* or *in vivo* efficiently induces expression of the αE integrin which complexes with integrin β7 to form $\alpha_E\beta_7$ (CD103) and binds to E-cadherin expressed by epithelial cells (Casey et al., 2012; Mackay et al., 2013; Sheridan et al., 2014; Wakim et al., 2015). Although Trm cell expression of CD103 is not universal across all tissues, in skin at least, CD103 expression is induced by Trm cell precursors upon entry to epidermis and, along with CD69, is a good phenotypic marker for Trm cells (Casey et al., 2012; Mackay et al., 2013). Ablation of CD103 in $CD8^+$ T cell prevents their long-term persistence in the epidermis (Mackay et al., 2013).

TGFβ is produced bound to the latency associate peptide that prevents bioactivity until the complex is activated (Worthington et al., 2011). In the epidermis, TGFβ activation is mediated exclusively by activation via the integrins $\alpha_v\beta_6$ and $\alpha_v\beta_8$ that are expressed by keratinocytes (KCs) (Aluwihare et al., 2009; Mohammed et al., 2016; Yang et al., 2007). Using a DNFB-pull Trm cell model in *Itgb6*$^{-/-}$*Itgb8*$^{\Delta KC}$ mice (*Itgb6*$^{-/-}$ x *Itgb8*$^{fl/fl}$-*Krt14-cre*) lacking both integrins in the skin, we have previously shown that $CD8^+$ T cell effectors are recruited into the epidermis at early time points, but Trm cells are not evident at late time points. In addition, blocking mAbs to $\alpha_v\beta_6$ could partially deplete fully differentiated Trm cells suggesting that continued access to integrin-activated TGFβ is required for persistence of epidermal Trm cells (Hirai et al., 2019; Mohammed et al., 2016). A formal demonstration that epidermal Trm cells require continued exposure to TGFβ, identification of the source of TGFβ supporting Trm cells and whether DNFB-pull bystander and antigen-specific Trm cells equally depend on TGFβ remain unexplored questions.

Herein, we show that fully differentiated epidermal Trm cells have an absolute dependence on TGFβ transactivated by $\alpha_v\beta_6$ and $\alpha_v\beta_8$ on KC for long-term persistence in the epidermis. In addition, the source of TGFβ supporting Trm cells was autocrine. We also found that both "antigen-specific" OT-I Trm cells generated by VV-OVA skin infection and bystander DNFB-pull Trm cells persisted long-term under steady-state conditions. However, when active-TGFβ was limited by administration of blocking $\alpha_v\beta_6$ and $\alpha_v\beta_8$ mAbs or by small molecule inhibition, antigen-specific Trm cells were able to persist in the epidermis while bystander Trm cells were depleted. Similarly, when new T cells were recruited into the skin by a subsequent challenge, antigen-specific Trm cells were better able to persist than bystander Trm cells. Genetically enforced TGFβR signaling rescued this phenotype and allowed bystander Trm cells to persist in the epidermis as efficiently as antigen-specific Trm cells in both contexts. Thus, we have found that Trm cells compete for integrin-activated TGFβ resulting in an unexpected selective pressure promoting the retention of antigen-specific Trm cells within the epidermal niche.

RESULTS

Epidermal Trm cells require TGFβ signaling for persistence

Despite strong evidence that active TGFβ is required for differentiation of $CD8^+$ T cell effectors into Trm cells, it remains unclear whether continued exposure to TGFβ is required for their persistence in skin. To directly test a requirement for TGFβ in the memory phase, 10^5 $CD8^+$ T cells from OT-I ROSA26-*creER*^{T2} x *Tgfbr2*$^{fl/fl}$ (Thy1.2/Thy1.2, CD45.2/CD45.2) and control OT-I ROSA26-*creER*^{T2} x *Tgfbr2*$^{f/+}$ (Thy 1.1/Thy1.2, CD45.1/CD45.2) mice were mixed and adoptively transferred into naïve C57BL/6 CD45.1 recipient mice (Figure 1A). Recipients were then infected with recombinant vaccinia virus expressing $OVA_{257–264}$ (VV-OVA) using the skin scarification method on the flank (Hirai et al., 2019). Equal expansion of OT-I was confirmed in blood (Figure 1B) and tamoxifen was administered i.p for 5 consecutive days starting on day 42 post-infection to ablate *Tgfbr2*. 23 days after tamoxifen treatment (day 70 post infection) the number of epidermal *Tgfbr2*$^{-/-}$ and sufficient OT-I was determined by immunofluorescent microscopic imaging of epidermal sheets. We enumerated epidermal Trm cells by direct immunofluorescent visualization because flow cytometry of enzymatically digested tissue greatly underestimates cell numbers in epidermis as well as other non-lymphoid tissues (Figure S1) (Collins et al., 2016; Steinert et al., 2015). Ablation of *Tgfbr2* resulted in a significant decrease in the number of epidermal Trm cells compared with control (Figure 1C). From these data we conclude that Trm cells require TGFβ signaling in order to maintain epidermal persistence at a late timepoint post infection well after differentiation has occurred. Thus, skin Trm cells depend on TGFβ at all stages of their development: naïve (Mani et al., 2019), transition of effectors to memory (Mackay et al., 2013; Mackay et al., 2015), as well as memory maintenance.

Epidermal Trm cells require integrin-activated TGFβ for persistence

We have previously reported using both a VV-infection model and a “DNFB-pull” bystander model that epidermal Trm cells are absent in *Itgb6*$^{-/-}$*Itgb8*$^{\Delta KC}$ mice that lack KC expression of the TGFβ-activating integrins $\alpha_v\beta_6$ and $\alpha_v\beta_8$ (Hirai et al., 2019; Mohammed et al., 2016). To clarify if the defect of Trm cells in *Itgb6*$^{-/-}$*Itgb8*$^{\Delta KC}$ mice results from failure of differentiation and/or maintenance, we performed a kinetic analysis of Trm cells in WT, *Itgb6*$^{-/-}$, or *Itgb6*$^{-/-}$*Itgb8*$^{\Delta KC}$ mice. We adoptively transferred 10^5 OT-I cells into naïve WT, *Itgb6*$^{-/-}$, or *Itgb6*$^{-/-}$*Itgb8*$^{\Delta KC}$ mice followed by VV-OVA skin scarification infection. The number of epidermal OT-I cells was quantified by immunofluorescent microscopy on days 14, 28, and 56 days post VV-OVA infection. OT-I numbers were greatly reduced in *Itgb6*$^{-/-}$*Itgb8*$^{\Delta KC}$ starting on day 14 post infection (Figure 1D and 1E). Trm cell number in *Itgb6*$^{-/-}$ were intact on day 14 but declined on days 28 and 56 compared to WT mice. The early absence of Trm cells in *Itgb6*$^{-/-}$*Itgb8*$^{\Delta KC}$ likely represents a failure of differentiation of Trm cells due to the absence of active TGFβ while the delayed loss observed in *Itgb6*$^{-/-}$ likely represents a failure of persistence when active TGFβ is limited. This is supported by the presence of OT-I cells that lack expression of the Trm cell marker CD103 in *Itgb6*$^{-/-}$*Itgb8*$^{\Delta KC}$ mice (Figure 1F and 1G). In addition, even though Trm cell developed in *Itgb6*$^{-/-}$ mice, expression of CD103 was reduced compared to Trm cells in WT mice indicating that amounts of CD103 expression reflect the amounts of available active TGFβ.

To formally confirm that loss of Trm cells in *Itgb6*$^{-/-}$ mice resulted from reduced amounts of active TGFβ, we bred *Itgb6*$^{-/-}$ mice to mice with CD8-specific expression of *cre*ER^{T2} (E8I-*cre*ER^{T2}) and mice expressing a constitutively active form of the TGFβ receptor I (TGFβRCA) behind a lox-stop-lox cassette (Bartholin et al., 2008; Hirai et al., 2019; Liu et al., 2020; Vincent et al., 2010). The resulting mice (*Itgb6*$^{-/-}$ x TGFβRCA) allow for tamoxifen (TAM)-induced expression of TGFβRCA in CD8^{+} T cells. *Itgb6*$^{-/-}$ x TGFβRCA^{CD8} mice and control *Itgb6*$^{+/-}$, *Itgb6*$^{-/-}$, and *Itgb6*$^{+/-}$ x TGFβRCA^{CD8} mice were infected with VV by skin scarification and treated with tamoxifen i.p. on days 7–11 post infection. On day 46 post infection, epidermal Trm cells were enumerated. As expected, Trm cell numbers and expression of CD103 were reduced in *Itgb6*$^{-/-}$ compared to *Itgb6*$^{+/-}$ mice (Figure 2A–D). Notably, in *Itgb6*$^{-/-}$ mice, tamoxifen-induced expression of TGFβRCA rescued Trm cell numbers and CD103 expression to amounts equivalent to those observed in control *Itgb6*$^{+/-}$ mice. Forced expression of TGFβRCA by CD8^{+} T cells in control *Itgb6*$^{+/-}$ mice increased expression of CD103 but did not increase Trm cell numbers. From these data we conclude that reduced expression of CD103 and reduced numbers of Trm cells in *Itgb6*$^{-/-}$ mice resulted from lower amounts of available active TGFβ.

Some groups have reported relatively low numbers of Trm cells in the ear and many of the Trm cells were observed to express little to no CD103 (Collins et al., 2016; Gamradt et al., 2019; Hobbs and Nolz, 2019; Slutter et al., 2017). This is in contrast with our data showing uniformly high expression of CD103 in the flank. We hypothesized that the skin sites infected (i.e. flank vs. ear) could explain this discrepancy. To test this hypothesis, OT-I adoptive transfer WT mice were dual infected with VV-OVA on both the ear and flank skin. On day 34 post infection, the number of OT-I was significantly greater in flank than ear skin (Figure 2E and 2F). This could have potentially resulted from altered viral infection efficiency except that we noticed Trm cells in ear skin consistently expressed lower amounts of CD103 suggesting reduced availability of active TGFβ (Figure 2G and 2H). Comparison of $\alpha_v\beta_6$ expression on KCs by flow cytometry and RTqPCR revealed lower expression in ear compared with flank skin (Figure 2I and S2). We did not observe differential expression of *Il7* or *Il15* mRNA (Figure S2) (Adachi et al., 2015; Mackay et al., 2013; Richmond et al., 2018). Finally, TGFβRCA^{CD8} were dual infected with VV on ear and flank followed by administration of tamoxifen i.p. starting on day 14. Analysis of epidermis 37 days after infection revealed that induction of constitutive TGFβR signaling significantly rescued Trm cell numbers in ear (Figure 2J and 2K). These data further support the concept that Trm cells are sensitive to amounts of available active TGFβ in the epidermis and that these amounts can vary between anatomical sites.

Epidermal Trm cells require autocrine TGFβ

Potential epidermal sources of TGFβ to support Trm cell persistence include keratinocytes (KC), Langerhans cells (LC), dendritic epidermal T cells (DETC), and Trm cells (Yang et al., 2019). Trm cells are unaffected by the absence of LC and DETC indicating these cell types are not obligate sources of TGFβ (Mohammed et al., 2016; Zaid et al., 2014). Since KC are the largest source of TGFβ in the epidermis (Yang et al., 2019), we hypothesized that KC-derived TGFβ is required to support Trm cells persistence. To test this, we used *Krt14-cre*ER^{T2} x *Tgfb1*$^{fl/fl}$ mice (*Tgfb*$^{\Delta KC}$) that allow for the inducible ablation of *Tgfb1* from

KCs. *Tgfb*$^{\Delta KC}$ mice also have a ROSA26-YFP reporter, which accurately reports *Tgfb1* ablation (Yang et al., 2019). *Tgfb*$^{\Delta KC}$ and control mice were infected with VV followed by topical application of 4-OH-tamoxifen on day 42 post infection. The epidermis was analyzed on day 63 post infection (21 days after tamoxifen). We observed that approximately 80% of KC expressed YFP (green) indicative of loss of *Tgfb1* (Figure 3A and 3B). Importantly, YFP^{-} KC were clustered together resulting in large YFP^{+} areas lacking *Tgfb1* expression. We observed that numbers of Trm cells (magenta) were unaffected by the absence of *Tgfb1* (Figure 3C) and were distributed equally throughout YFP^{+} and YFP^{-} areas (Figure 3A) indicating that KC-derived TGFβ is not required for Trm cell persistence.

We next examined whether Trm cell persistence requires autocrine TGFβ. We bred E8I-*cre*ER^{T2} mice with a human nerve growth factor receptor reporter (hNGFR) and *Tgfb1*$^{fl/fl}$ mice. The resulting *Tgfb*$^{\Delta CD8}$ mice allow for tamoxifen-inducible ablation of *Tgfb1* from CD8^{+} T cells that can be monitored by expression of hNGFR. *Tgfb*$^{\Delta CD8}$ and control hNGFR^{CD8} mice were infected with VV followed by i.p tamoxifen for 5 consecutive days starting on day 42 post infection. Epidermal sheets were evaluated by immunofluorescent microscopy for expression of CD8α (magenta) to identify all Trm cells and hNGFR (yellow) to identify those Trm cells that had successfully undergone *cre*-mediated excision. We observed that tamoxifen-mediated *cre* activation with hNGFR expression was observed in approximately 50% Trm cells in control hNGFR^{CD8} mice. The number of hNGFR^{+} CD8^{+} Trm cells in *Tgfb*$^{\Delta CD8}$ mice, however, was significantly reduced compared with control mice (Figure 3D and 3E). Notably, hNGFR^{-} and hNGFR^{+} Trm cells were observed in close proximity to each other in control hNGFR^{CD8} mice but in *Tgfb*$^{\Delta CD8}$ mice, hNGFR^{-} Trm cells were unaffected. Thus, we conclude that epidermal Trm cells are dependent on an autocrine source of TGFβ to maintain epidermal persistence.

Blockade of integrin-mediated TGFβ activation eliminates bystander Trm cells

As discussed above, antigen-specific Trm cells generated by VV skin infection and bystander Trm cells generated by a “DNFB-pull” are both absent from *Itgb6*$^{-/-}$*Itgb8*$^{\Delta KC}$ mice which lack integrin-mediated TGFβ activation. To test whether antigen-specific and bystander Trm cells are equally dependent on integrin-activated TGFβ, we compared the ability of VV-induced Trm cells and DNFB-pulled Trm cells to persist following administration of blocking anti-$\alpha_v\beta_6$ and $\alpha_v\beta_8$ mAbs. Thy1.1^{+} OT-I cells were adoptively transferred into naïve WT mice followed by skin VV-OVA infection on left flank skin. On day 5 post infection, the right flank was painted with DNFB to recruit expanded OT-I effectors into the site. Mice were injected weekly with anti-$\alpha_v\beta_6$ and $\alpha_v\beta_8$ mAbs starting on day 42–49 post infection for a total of 3 weeks followed by immunofluorescent microscopic evaluation of epidermal whole mounts (Figure 4A). As a positive control, we stained for MHC-II (green) to identify Langerhans cells and observed the expected reduction following administration of anti-$\alpha_v\beta_6$ and $\alpha_v\beta_8$ at VV-OVA, DNFB-pulled and non-treated (NT) sites (Figure 4B and 4C) (Mohammed et al., 2016). VV-OVA infection and DNFB-pulled treatment induced Trm cells (Thy1.1, cyan) to the sites in equal number and much more than NT sites. We observed a sizable reduction in the number of Trm cells in anti-$\alpha_v\beta_6$ and $\alpha_v\beta_8$ treated animals at the DNFB-pulled and NT sites but not at the VV-OVA sites. Notably, expression of CD103 was reduced in Trm cells at both in VV-OVA and DNFB-pulled

indicating an equivalent reduction in available active TGFβ at both sites (Figure 4D). We obtained similar results using CWHM-12, a small molecule $\alpha_v\beta_6$ and $\alpha_v\beta_8$ inhibitor (Figure 4E and 4F) (Henderson et al., 2013). The loss of Trm cells from the VV-OVA site seen in *Itgb6*$^{-/-}$ mice but not following anti-$\alpha_v\beta_6$/$\alpha_v\beta_8$ or CHWM12 treatment likely resulted from only partial inhibition of integrin-mediated TGFβ activation by these agents. In the absence of TGFβ-blockade, Trm cells at both sites appeared functionally equivalent and were able to persist in the epidermis under steady state conditions for up to 460 days (Figure S3). To determine whether the lowered sensitivity to limiting amounts of TGFβ at the VV-OVA sites was related to viral-induced local inflammation, we repeated the experiment by dual infecting mice with VV-OVA and recombinant VV expressing an irrelevant antigen (nucleocapsid protein of vesicular stomatitis virus, VV-N) on opposite flanks. As expected, the number of OT-I cells at the VV-N infected sites was significantly lower than the VV-OVA sites due to antigen-mediated competition with endogenous VV-N-specific CD8$^+$ T cells (Figure 4G and 4H) (Khan et al., 2016; Muschaweckh et al., 2016). Importantly, following administration of anti-$\alpha_v\beta_6$ and $\alpha_v\beta_8$, bystander OT-I cells at the VV-N sites were depleted but OT-I cells at the VV-OVA sites were unaffected. Thus, from these data we conclude that antigen-specific OT-I cells at the VV-OVA sites are better able to persist in the epidermis than bystander OT-I cells at either DNFB-pulled, NT, and VV-N sites under conditions where integrin-mediated TGFβ activation is limited.

We next sought to test the hypothesis that encounter with antigen in the skin renders Trm cells more resistant to limiting amounts of active TGFβ. WT OT-I adoptive transfer mice were infected with VV-OVA on the left flank followed by epicutaneous application of DNFB on day 5 post-infection (Figure 4I). One day later the DNFB-pulled sites were painted with $OVA_{257–264}$ peptide. On Day 42, mice were treated with CWHM-12 or control for 4 weeks to inhibit integrin-mediated TGFβ activation. Addition of cognate antigen to the DNFB-pulled sites now made Trm cells at these sites behave similar to Trm cells at the VV-OVA sites as they persisted in the epidermis despite inhibition of TGFβ activation (Figure 4J). From these data we conclude that under conditions of limiting amounts of active TGFβ created by either blocking mAbs or small molecule inhibition, Trm cells that have encountered cognate antigen in the skin are better able than bystander Trm cells to persist in the epidermis.

TGFβ signaling provides a competitive advantage during Trm cell development

Since access to active TGFβ is required for Trm cells to establish in the epidermis and antigen-specific Trm cells are better able to persist during the memory phase than bystander Trm cells when amounts of active TGFβ are limited, we hypothesized that competition for active TGFβ may provide a selective pressure during the development of Trm cells. To test this hypothesis, we generated OT-I x TGFβRCA^{CD8} mice. CD8$^+$ T cells from these or control OT-I mice were adoptively transferred into WT recipients and dual infected with VV-OVA and VV-N on opposite flanks (Figure 5A). Mice were treated with tamoxifen i.p for 5 days starting on day 7 post-infection and the epidermis was analyzed on day 34 post-infection for the presence of OT-I (Thy1.1, cyan) and endogenous (CD8α, red) Trm cells (Figure 5B). As expected, large numbers of OT-I Trm cells were evident in control mice at the VV-OVA sites but these cells were out competed by endogenous VV-specific Trm cells at

the VV-N sites (Figure 5B and 5C). OT-I TGFβRCA^{CD8} formed Trm cells as efficiently as control OT-I at the VV-OVA sites where cognate OVA antigen was available. Importantly, at the VV-N sites where OVA antigen is absent, OT-I TGFβRCA^{CD8} Trm cells were able to effectively compete with endogenous Trm cells resulting in equivalent numbers of endogenous and OT-I TGFβRCA^{CD8} Trm cells. At the non-treated (NT) sites where the Trm cells are sparse and there is less inter-clonal competition, constitutive TGFβR signaling did not provide a competitive advantage. From these data we conclude that enforced TGFβR signaling is able to overcome the competitive advantage provided by antigen encounter in skin during Trm cell development. This suggests that competition for active TGFβ can participate in determining which clones occupy the epidermal niche.

Bystander Trm cells are preferentially displaced by newly recruited CD8$^+$ T cells

If Trm cell clones compete for active TGFβ in order to persist in the epidermis, then one prediction is that bystander Trm cells will compete less efficiently than antigen-specific Trm cells when new CD8$^+$ T cells are recruited into the skin during a subsequent challenge. To test this prediction, WT OT-I adoptive transfer mice were infected with VV-OVA on one flank followed by a DNFB-pulled on the opposite flank to establish antigen specific and bystander Trm cell sites, respectively (Figure 6A). After at least 40 days post-infection, mice were sensitized at a distant sites (abdomen) with the hapten oxazolone which is antigenically distinct from DNFB to generate oxazolone-specific effectors (Kish et al., 2009). Oxazolone effectors were then recruited into both the VV-OVA and DNFB-pulled sites by epicutaneous application of oxazolone. At least 30 days after oxazolone challenge, the epidermis at the VV-OVA and DNFB-pulled sites were analyzed. As noted earlier, without the oxazolone challenge equivalent numbers of OT-I Trm cells developed at the VV-OVA and DNFB-pulled sites (Figure 6B and 6C). Challenge with oxazolone, however, reduced the numbers of OT-I at both sites, but numbers of OT-I Trm cells at the DNFB-pulled sites were consistently lower than at the VV-OVA sites. This suggests that Trm cells at the VV-OVA sites were better able than Trm cells at the DNFB-pulled sites to compete with the newly recruited endogenous CD8$^+$ T cells. To ensure that this is a result of competition between Trm cells and is not reflective of recruited circulating OT-I cells, we repeated the experiment but depleted circulating OT-I cells by injecting titrated anti-Thy1.1 just prior to oxazolone challenge (Figure S4). In the absence of circulating OT-I cells, we observed a similar phenotype where OT-I Trm cells at the VV-OVA sites are better able to compete with newly recruited T cells than OT-I Trm cells at the DNFB-pulled sites (Figure 6E). In addition, if the DNFB-pulled sites was treated with OVA$_{257–264}$ during the initial seeding (day 6 p.i.), then Trm cells at this location showed a similar capacity as Trm cells at the VV-OVA sites to compete with newly recruited T cells (Figure 6E). Thus, Trm cells that have encountered Ag in the skin during initial Trm cell formation are better able to persist in the context of a subsequent challenge when new T cells are recruited into the skin.

We repeated this experiment to analyze the epidermis at an earlier timepoint—day 10 post-oxazolone challenge—in order to better visualize clonal competition when Trm cell differentiation is still occurring. In addition, to determine whether loss of OT-I cells following oxazolone-challenge required recruitment of CD8$^+$ T cells, we depleted all circulating CD8$^+$ T cells by titrated anti-CD8β antibody before oxazolone challenge (Figure

7A and Figure S4). As expected, in control mice treated with anti-Thy1.1 to deplete circulating OT-I cells, we observed a large influx of endogenous $CD8^+$ T cells at both VV-OVA and DNFB-pulled sites. Numbers of OT-I Trm cells at the DNFB-pulled were decreased but not at the VV-OVA sites (Figure 7B and 7C). In mice treated with anti-CD8β antibody, recruited endogenous T cells were not observed and, importantly, numbers of OT-I Trm cells were not reduced indicating that competition from newly recruited $CD8^+$ T cells drives the loss of OT-I cells. Furthermore, we observed significant decrease of CD103 expression by OT-I Trm cells from both oxazolone VV-OVA and DNFB-pulled sites that did not occur in mice treated with anti-CD8β antibody (Figure 7D). These data suggest that when newly recruited $CD8^+$ T cells enter the epidermis, the amount of available active TGFβ is reduced and that competition for active TGFβ is a key factor determining persistence of Trm cells.

To determine whether competition for active TGFβ determines persistence of established Trm cells when new $CD8^+$ T cells are recruited, we repeated the above experiment but compared OT-I with OT-I TGFβRCA^{CD8} Trm cells (Figure 7E). $CD8^+$ T cells from OT-I or OT-I TGFβRCA^{CD8} mice were adoptively transferred into WT recipients. Trm cells were established using VV-OVA followed by a DNFB-pull on opposite flanks. Mice were then treated on day 42 post-infection with tamoxifen i.p. followed by oxazolone sensitization on the abdomen and challenge on VV-OVA and DNFB-pulled sites. The epidermis was analyzed at least 30 days following oxazolone challenge. As before, we observed that oxazolone challenge reduced numbers of OT-I Trm cells but numbers of OT-I TGFβRCA^{CD8} Trm cells were largely intact following oxazolone challenge (Figure 7F and 7G). Thus, forced TGFβR signaling allows Trm cells to better compete with newly recruited $CD8^+$ T cells. From these data we conclude that competition for active TGFβ is a key factor determining epidermal residency of Trm cells.

To explore molecular pathways that could facilitate the increased persistence of antigen-specific over bystander Trm cells in the epidermal niche, we performed RNA-seq analysis on paired epidermal OT-I Trm cells that were FACS sorted from the VV-OVA or DNFB treated sites of individual WT animals at 57–70 days after infection. The paired analysis revealed 100 differentially expressed genes (DEGs) (RPKM>4, p-value<0.05, $\log_2$FC>0.58) (Table S1). These DEGs did not include any in the TGFβ signaling pathway (Figure S5). In addition, gene ontology (GO) enrichment analysis of the DEGs did not identify alteration in TGFβ-associated pathways. Notably, expression of histone variants associated with chromosome silencing and chromosome organization was increased in bystander Trm cells. Thus, antigen-specific and bystander Trm cells manifest highly similar transcriptionally states but may have epigenetic differences that could determine their differing capacity to persist when active TGFβ becomes limited.

DISCUSSION

In summary, we demonstrated that long-term epidermal persistence of Trm cells under steady-state conditions requires intrinsic TGFβR signaling, autocrine TGFβ, and TGFβ transactivation by integrin $\alpha_v\beta_6$ and $\alpha_v\beta_8$ expressed on KC. We also showed that when integrin-mediated TGFβ activation is impaired by mAbs or small molecule blockade,

antigen-specific Trm cells persist in the epidermis while bystander Trm cells are partially depleted. Similarly, when new $CD8^+$ effectors are recruited into the epidermis, expression of CD103 on Trm cells is decreased indicative of a reduced availability of active TGFβ and bystander Trm cells are preferentially replaced by newly recruited $CD8^+$ T cells. In both contexts, forced TGFβR signaling was sufficient to rescue bystander Trm cells. Based on these data we propose a model in which access to active TGFβ in the epidermis is a key factor in determining successful colonization of the epidermal niche by Trm cells and intraclonal competition for active TGFβ represents an unappreciated mechanism to preferentially enrich antigen-specific clones at the skin barrier.

The importance of TGFβ and TGFβ-induced CD103 for development of skin Trm cells has been well demonstrated using adoptive transfer of the gene deficient $CD8^+$ T cells (Mackay et al., 2013). By conditionally ablating *Tgfbr2* after epidermal Trm cell differentiation and by demonstrating that forced TGFβR signaling retains Trm cells in $\alpha_v\beta_6$-deficient mice, we now formally demonstrate that ongoing TGFβ signaling is required for maintenance of Trm cells in the epidermis. During the memory phase, Trm cells depend on transactivation of autocrine TGFβ. We favor an autocrine over a paracrine mechanism since physically adjacent Trm cells that had not excised *Tgfb1* were not affected by the loss of *Tgfb1* by their neighbors. Naïve $CD8^+$ T cells also require TGFβ activation by α_v-expressing integrins expressed on DC in lymph nodes to maintain Trm cell differentiation potential (Mani et al., 2019). This parallel and the dependence of Trm cells on TGFβ at all stages of development suggests that transactivation of autocrine TGFβ may also be required by naïve and effector cells. LC and regulatory T (Treg) cells also depend on autocrine TGFβ (Bobr et al., 2012). Treg cells express glycoprotein-A repetitions predominant protein (GARP) that binds surface autocrine TGFβ (Tran et al., 2009). $CD8^+$ Trm cells, however, express low amounts of *GARP* but relatively high amounts of a *GARP* homologue, *Lrrc33* (Mackay et al., 2013; Pan et al., 2017; Qin et al., 2018) (Figure S5). We speculate that LRRC33 may participate in binding autocrine TGFβ on Trm cells thereby facilitating transactivation.

The enhanced ability of antigen-specific Trm cells at the VV-OVA sites compared to bystander Trm cells at the DNFB-pulled sites to persist in the epidermis when new $CD8^+$ T cells are recruited by oxazolone indicates that encounter to cognate antigen in the epidermis renders Trm cells more fit and better able to compete with new immigrants. The data indicating that it is competition for TGFβ comes from the observations that expression of CD103 is reduced on Trm cells shortly after oxazolone challenge only when $CD8^+$ T cells are recruited into the skin but not when this is prevented by administration of anti-CD8β. In addition, forced expression of TGFβR signaling allowed bystander Trm cells to compete with newly recruited $CD8^+$ T cells as efficiently as antigen-specific Trm cells. Moreover, when forced TGFβR signaling occurred during Trm cell differentiation, bystander OT-I recruited into a site without antigen (VV-N) were better able to compete with endogenous T cells. Thus, competition for active TGFβ appears to occur both during memory and during Trm cell differentiation. This suggests that competition for TGFβ is a mechanism to preferentially maintain antigen-specific over bystander Trm cells in the epidermis during sequential challenges. It may also participate in the enrichment of antigen-specific Trm cells during an initial challenge to naïve skin.

To explore why antigen-specific Trm cells have a competitive advantage over bystander Trm cells when active TGFβ is limited, we compared their transcriptional states. Somewhat unexpectedly, we found both types of Trm cells to manifest highly similar transcriptional states, including genes associated with the TGFβ signaling pathway. This is consistent with the observation that both bystander and antigen-specific Trm cells show a similar reduction of CD103 expression when new T cells are recruited into the skin, indicative of reduced access to active TGFβ due to competition. A key difference between antigen-specific and bystander Trm cells is that the former encounter cognate antigen in the epidermis that activates TCR signaling. The importance of a secondary TCR signaling input in distinguishing the cellular fate dynamics of antigen-specific and bystander Trm cells after their arrival in the epidermis is reinforced by the observations that 1) antigen encounter in the epidermis results in a durable alteration in Trm cells and 2) exposure of bystander Trm cells to cognate antigen in the epidermis enables them to persist despite inhibition of TGFβ activation. The RNA-seq analysis of antigen-specific and bystander Trm cells revealed histone gene variants associated with chromosome silencing and chromosome organization that were more highly expressed in bystander Trm cells. Collectively, these findings lead us to propose that antigen-specific and bystander Trm cells may not differ in their TGFβ sensing and TGFβR signaling capacities but rather that the presence or absence of TCR stimulation during their transition into the tissue-resident memory state may drive distinct epigenetic changes that affect their capacity to persist when active TGFβ becomes limiting.

An implication of our model is that the epidermis represents an environmental niche capable of maintaining a finite number of Trm cells possibly driven by limited physical space or survival factor(s). Circulating memory T cells can be sequentially expanded through multiple rounds of heterologous prime-boost immunizations (Vezys et al., 2009). In contrast, we do not observe expanded numbers of Trm cells following a subsequent challenge with oxazolone suggesting that the epidermis can support a finite number of T cells. This is consistent with previous reports showing that Trm cells replace DETC to maintain an invariable number of total epidermal T cells (Zaid et al., 2014) and that adoptive transfer of increasing numbers of *in vitro* activated T cells pulled by DNFB to skin does not increase Trm cells numbers beyond a set limit (Park et al., 2018). It is unlikely that the epidermal niche size is determined by active TGFβ since forced TGFβR signaling in T cells augmented intraclonal competition but did not increase overall numbers of epidermal Trm cells. Rather, we speculate that the epidermal niche is determined either by limitations of physical space or by limited amounts of T cell survival and/or homeostatic proliferation factors such as IL-7 or IL-15 (Adachi et al., 2015; Richmond et al., 2018). It remains unclear whether a limited niche exists only in the epidermis or whether it extends to other compact monolayers such as the intestinal epithelium, or solid organs and stromal compartments as well. We note that expression of CD103 by Trm cells is not universal and is relatively enriched in barrier epithelia like epidermis and intestinal epithelium (Steinert et al., 2015). The high frequency of $CD103^{-}$ Trm cells in tissues such as liver suggests that T cell competition for active TGFβ may be limited to certain barrier epithelia.

In conclusion, T cell competition for transactivated autocrine TGFβ participates in shaping the epidermal niche. Though we have focused exclusively on epidermal Trm cells, we think it is likely that a similar mechanism occurs in other active TGFβ-rich tissues where Trm

cells express high amounts of CD103. In addition, we have focused on T cells recruited to the skin by transient infection or sensitizing hapten. Whether or not this mechanism also occurs in the context of chronic antigen such as in the tumor micro-environment or commensal-specific T cells and an exploration into the possible epigenetic alterations that distinguish bystander from antigen-specific Trm cells remain to be explored.

STAR METHODS

RESOURCE AVAILABILITY

Lead Contact—Further information and requests for resources and reagents should be directed to and will be fulfilled by the Lead Contact, Daniel H. Kaplan (dankaplan@pitt.edu).

Materials Availability—This study did not generate new unique reagents.

Data and Code Availability—The RNA-seq datasets reported in this paper can be found at GEO: GSE156668.

EXPERIMENTAL MODEL AND SUBJECT DETAILS

Mice—*Itgb6*$^{-/-}$ and *Itgb8*^{loxP} mice were kindly provided by Dean Sheppard (University of California, San Francisco). E8I-*cre*ER^{T2} and ROSA26.LSL.hNGFR reporter mice were developed by Dario A.A. Vignali (University of Pittsburgh) (Hirai et al., 2019). *Tgfb*^{loxP} and TGFβRICA mice have been previously described (Bartholin et al., 2008; Liu et al., 2020; Marie et al., 2006). C57BL/6 (WT), B6.SJL-Ptprca Pepcb/BoyJ (CD45.1), Tg(KRT14-cre)1Amc/J (*Krt14-cre*), C57BL/6-Tg(TcraTcrb)1100Mjb/J (OT-I), B6.129S7-Rag1tm1Mom/J (Rag$^{-/-}$), CBy.PL(B6)-Thy1^{a}/ScrJ (Thy1.1) mice were purchased from Jackson Laboratories. We crossed *Krt14-cre* mice with *Itgb8*^{loxP} and *Itgb6*$^{-/-}$ mice to obtain *Itgb6*$^{-/-}$ *Itgb8*$^{\Delta KC}$ mice (Mohammed et al., 2016). E8I-*cre*ER^{T2} mice were crossed with TGFβRI-CA mice to obtain TGFβRICA^{CD8} mice. TGFβRI-CA^{CD8} mice were further crossed with *Itgb6*$^{-/-}$ mice to generate *Itgb6*$^{-/-}$ x TGFβRI-CA^{CD8} mice. E8I-*cre*ER^{T2} mice were crossed with ROSA26.LSL.hNGFR reporter mice and *Tgfb*^{loxP} mice to obtain *Tgfb*$^{\Delta CD8}$ mice. *Krt14-cre*ER^{T2} mice were bred with *Tgfb*^{loxP} mice and ROSA26.LSL.YFP (Jackson Laboratories) reporter mice resulting *Tgfb*$^{\Delta KC}$ mice. We generated Thy1.1^{+}Rag$^{-/-}$OT-I mice by crossing OT-I mice with Rag$^{-/-}$ and Thy1.1 mice. TGFβRICA^{CD8} mice and Thy1.1^{+}Rag$^{-/-}$OT-I mice were bred to generate OT-I TGFβRI-CA mice. OT-I cells carrying ROSA26-*cre*ER^{T2} and floxed TGFβ receptor II gene (OT-I *cre*ER^{T2} TGFbRII$^{fl/fl}$) were kindly provided by Thorsten Mempel (Harvard University). We used age- and sex-matched (males and female) mice that were between 6 and 12 weeks of age in all experiments. All mice were maintained under specific-pathogen-free conditions and all animal experiments were approved by University of Pittsburgh Institutional Animal Care and Use Committee.

METHOD DETAILS

Trm cell models and blocking TGFβ activation treatments—Mice were infected by skin scarification (skin infection) with 3×10^6 plaque-forming units recombinant vaccinia virus expressing the SIINFEKL peptide of ovalbumin (VV-OVA). For skin scarification, 45

μL of VV was applied to shaved left flank (4–5 cm^2) and the skin were gently scratched 100 times with 27 G needle under anesthesia. In some experiment, 3×10^6 plaque-forming units recombinant vaccinia virus expressing the nucleocapsid protein of vesicular stomatitis virus (VV-N) were applied to shaved right flank at the same day of VV-OVA infection. In some experiments VV-OVA infected mice were further treated with 0.15% 1-Fluoro-2,4-dinitrobenzene (DNFB, D1529: Sigma-Aldrich) in 4:1 acetone : olive oil (Sigma-Aldrich) on the flank opposite the site of infection (40 μL) 5 days post infection. In some experiments, 4:1 acetone and olive oil was added to the stock solution of $OVA_{257–264}$ (Anaspec, Fremont, CA) in DMSO (D2650, Sigma-Aldrich) (10 mg/mL) for a final concentration of $OVA_{257–264}$ at 0.2 mg/mL and 50 μL was painted to the DNFB-treated skin 1 day after DNFB-treatment. For blocking of TGFβ activation by antibodies, anti-$\alpha_v\beta_6$ (6.3g9) and anti-$\alpha_v\beta_8$ (ADWA-11) (kindly provided by Dean Sheppard) or Vehicle (PBS) were administered i.p. at a dose of 200 μg/mouse weekly for up to 3 weeks. For blocking TGFβ activation with a small molecule integrin inhibitor, compound CWHM-12 (kindly provided by Indalo therapeutics, Cambridge, MA) was solubilized in 100% DMSO. Further dilution to 50% DMSO was made in sterile PBS and dosed to 100 mg per kg body weight per day for 28 days. CWHM-12 or vehicle (control) was delivered by implantable ALZET osmotic minipumps (model 2004, Durect, Cupertino, CA). For sensitization of 4-Ethoxymethylene-2-phenyl-2-oxazolin-5-one (Oxazolone, 862207: Sigma-Aldrich), 40 μL of 20 mg/mL Oxazolone (in 4:1 acetone : olive oil) was administered twice with 5 days interval to shaved abdomen of Trm cell mice. For challenge, mice were received 40 μl Oxazolone (10 mg/mL 4:1 acetone : olive oil)/each side of shaved flank. In some experiment (Figure 2D–2J), mice infected VV-OVA on left flank were also infected with 1×10^6 VV-OVA (15 μL) on left ear on the same day as flank infection.

Adoptive transfers—OT-I cells were purified from spleen and lymph nodes by MojoSort Mouse CD8 T Cell Isolation Kit (Biolegend) according to the manufacturer's instructions and 1×10^5 OT-I cells were intravenously transferred is all experiments. All mice were allowed to rest for 1 day before further experimentation.

Tamoxifen treatment—Tamoxifen (T5648; Sigma-Aldrich) was dissolved in 1/10th volume of 200 proof ethanol following incubation at 37 °C for 15–30 min with 300 rpm shaking. Corn oil (Sigma-Aldrich) was added for a final concentration of Tamoxifen at 10 mg/ml and was administered to mice for 5 consecutive days by intraperitoneal injection at 0.05 mg per g body weight. 5 mg of 4-Hydroxytamoxifen (4-OH tamoxifen) (H7904–5MG; Sigma-Aldrich) was dissolved in 1.25 mL ≥99.5% acetone following incubation at 37 °C for 5–10 min with occasional vortexing. Corn oil (Sigma-Aldrich) was added for a final concentration of 2 mg/mL and was administered to mice for 2 consecutive days by topical application (40 μL/shaved left flank).

Immunofluorescence of epidermis—Epidermal sheets were prepared as previously described (Mohammed et al., 2016). Briefly, epidermal side of shaved defatted flank skin or splitted ear skin was affixed to slides with double-sided adhesive (3M, St. Paul, MN). Slides were incubated in 10 mM EDTA in PBS for 90 min at 37°C, followed by physical removal of the dermis. The epidermal sheets were fixed in 4% PFA at RT for 15 min. The eidermal

sheets were blocked with PBS containing 0.1% tween-20, 2% BSA and 2% rat serum or rabbit serum for 1 hour at RT before staining 1hour with antibodies at RT in PBS containing 0.1% tween-20 and 0.5% BSA. The slides were mounted with ProLong™ Gold Antifade Mountant (Thermo). Images were captured on an IX83 fluorescent microscope (Olympus Tokyo, Japan) using a x10 objective; image analysis was performed using cellSens Dimension software (Olympus). For enumeration of cells, three images from distant sites within an epidermal sheet from a mouse were counted (total 3 mm^2) manually or automatically in ImageJ64 after image processing by Adobe Photoshop (version 6) and the average number per mm^2 epidermis was calculated as representative of the epidermal sheet. Anti-CD45.2 (104), CD8α (53–6.7), Thy1.1 (OX-7), MHCII (M5/114.15.2), hNGFR (ME20.4), YFP (FM264G) were purchased from Biolegend.

Flow cytometry—Preparation of single cells suspension from tissues were performed as previously described (Mohammed et al., 2016). Briefly, for preparing single cells suspension from the epidermis, shaved skin was harvested and fat tissues was removed mechanically by forceps. Float their dermal side down in the Petri dish containing pre-warmed 37°C 0.3% trypsin (Sigma-Aldrich) solution in 150 mM NaCl, 0.5 mM KCl and 0.5 mM glucose. Incubate in CO_2 incubator at 37° for 50–60 minutes. The epidermis was physically separated from the dermis and disrupted by mincing and vigorous pipetting in RPMI1640 (Gibco, Grand Island, NY) with 0.02 M HEPES (Sigma-Aldrich), and 10% FBS (Hyclone). The resulting cells were filtered through a 40 μm cell strainer (BD Biosciences). Blood were collected with heparin (Sigma-Aldrich) and treated with red blood cell lysing buffer (Sigma-Aldrich). Single-cell suspensions were blocked with 2.4G2 culture supernatant (American Type Culture Collection) and were stained with antibodies to extracellular markers and Fixable Viability Dye (eFluor 780) (eBioscience) in PBS with 2% FBS (Hyclone) and 0.05% Azide for 15 min at 4°C. For intracellular cytokines and Granzyme B staining, cells were fixed and permeabilized with Cytofix/Cytoperm kit (BD Biosciences) according to the manufacturer's instructions. Anti- CD8α (53–6.7), CD44 (IM7), TCRβ (H57–597), CD3 (17A2), Thy1.2 (30-H12), Thy1.1 (OX-7), granzyme B (GB11), CD69 (H1.2F3), CD103 (2E7), CD45.1 (A20), CD45.2 (104), IL-2 (JES6–5H4), and TNF-α (MP6-XT22) were purchased from Biolegend. Anti-CD8α (53–6.7), CD44 (IM7), CD69 (H1.2F3) and Thy1.1 (OX-7) were purchased from BD Biosciences. Anti-IFN-γ (XMG1.2) was purchased from TONBO bioscience (San Diego, CA). A BD LSRFORTESSA (BD Biosciences) and Flowjo software (TreeStar, Ashland, OR) were used for analysis. Enumeration of cells by flow cytometry was made by adding AccuCheck Counting Beads (Thermo Fisher) to samples.

RTqPCR—Epidermis from ear or flank skin was separated from dermis as described for the flow cytometry. The epidermis was minced finely with scissors and processed using the Qiagen RNeasy mini Kit (Thermo Fisher Scientific) following the manufacturer's instructions. RNA to cDNA conversion was performed using a High Capacity cDNA Reverse Transcription Kit (Applied Biosystems, Carlsbad, CA). cDNA was analyzed for *Intb6*, *Il7*, and *Il15* using TaqMan Gene Expression assays. Expression amounts of each gene were normalized to *Gapdh*.

***In vivo* recall response—**$OVA_{257–264}$ was purchased from Anaspec and the stock solution was prepared in DMSO (10 mg/mL) (D2650, Sigma-Aldrich). 4:1 acetone and olive oil was added for a final concentration of $OVA_{257–264}$ at 1 mg/mL and 50 μL was painted to each shaved skin sites of Trm cell mice. 10 mg/ml stock solution of Brefeldin A (B6542, Sigma-Aldrich) was prepared in DMSO. Further dilution to 0.5 mg/mL was made in PBS, and 500 μL was injected i.p. 6 hours after topical $OVA_{257–264}$ challenge. The skin was harvested 12 hours after the challenge and single suspension of epidermal cells were prepared as described above in the presence of Brefeldin A (2.5 μg/mL) for flow cytometry.

Circulating $CD8^+$ T cells depletion—For depletion of circulating memory OT-I cells, Oxa-sensitized Trm cell mice were injected i.p. with 0.3–1 μg anti-Thy1.1 (HIS51; ThermoFisher) in 200 μL PBS for 2 consecutive days before Oxa challenge. For depletion of circulating total $CD8^+$ T cells, mice were injected i.p. with 10 μg anti-CD8β (H35–17.2; ThermoFisher) in 200 μL PBS for 2 consecutive days before Oxa challenge. Depletion of OT-I or total $CD8^+$ T cells (≤ 0.5% of total $CD8^+$ T cells and ≤ 1% of $TCR\beta^+$ T cells, respectively) were confirmed by staining with anti-Thy1.1 (OX-7) or anti-CD8α (53–6.72), respectively using blood 3 days after Oxa challenge.

RNA-seq—Single cell suspension from VV-OVA infected or DNFB-treated epidermis 57–70 days after the infection from the same animal were prepared as described above. Samples from 2 animals were pooled to form a single sample. Live $CD45^+$ $Thy1.2^-$ $Thy1.1^+$ OT-I Trm cells were double FACS sorted to ensure high purity and directly lysed using the Clontech SMART-Seq v.4 kit for complimentary DNA synthesis. 200–1000 OT-I cells were collected in 12.5 uL of the lysis buffer. mRNA libraries were generated using Illumina Truseq Stranded mRNA Library Prep kit, followed by 75bp single indexed sequencing on an Illumina NextSeq500 to obtain 40–50 million reads per sample. RNA-seq analysis was performed as described previously (Chaudhri et al., 2020). Reads were mapped on mm9 genome assembly using Tophat2 (Kim et al., 2013; Langmead and Salzberg, 2012). Transcript abundances were calculated using cufflinks (Trapnell et al., 2010) as Reads Per Kilobase of transcript, per Million mapped reads (RPKM). RPKM values were imported in R and transformed as log2(RPKM+1). A paired t-test was then performed on this log transformed RPKM values. Genes with 50 percent fold increase or decrease ($log_2FC>0.58$) with p-values<0.05 were considered differentially expressed and subjected to conditional gene ontology enrichment analysis using “GOstats” package (Falcon and Gentleman, 2007).

QUANTIFICATION AND STATISTICAL ANALYSIS

Groups were compared with Prism software (GraphPad) using the two-tailed unpaired Student’s t test for comparison of two groups or Dunnett’s test for comparisons of more than two groups with the control. Data are presented as each data point and mean or mean ± standard error of the mean (s.e.m.). $p < 0.05$ was considered significant.

Supplementary Material

Refer to Web version on PubMed Central for supplementary material.

Acknowledgments

We thank Kate M. Vignali and Andrea L. Workman for constructing E8I-*cre*ER^{T2} and ROSA26.LSL.hNGFR reporter mice. We thank the members of the Kaplan and Vignali laboratory and members throughout the departments of Dermatology and Immunology for helpful discussions. We also thank the Division of Laboratory Animal Resources of the University of Pittsburgh for excellent animal care. The graphical abstract was created with BioRender.com. This work benefitted from SPECIAL BD LSRFORTESSATM funded by NIH 1S10OD011925-01.TH was supported by JSPS Overseas Research Fellowships; JDC by NIH T32 AI089443, AR060744S1; JDC by NIH T32AI089443; DHK by NIH R01AR060744; DAAV by NIH P01AI108545

References

Adachi T, Kobayashi T, Sugihara E, Yamada T, Ikuta K, Pittaluga S, Saya H, Amagai M, and Nagao K (2015). Hair follicle-derived IL-7 and IL-15 mediate skin-resident memory T cell homeostasis and lymphoma. Nat Med 21, 1272–1279. [PubMed: 26479922]

Allan RS, Smith CM, Belz GT, van Lint AL, Wakim LM, Heath WR, and Carbone FR (2003). Epidermal viral immunity induced by CD8alpha+ dendritic cells but not by Langerhans cells. Science 301, 1925–1928. [PubMed: 14512632]

Aluwihare P, Mu Z, Zhao Z, Yu D, Weinreb PH, Horan GS, Violette SM, and Munger JS (2009). Mice that lack activity of alphavbeta6- and alphavbeta8-integrins reproduce the abnormalities of Tgfb1- and Tgfb3-null mice. J Cell Sci 122, 227–232. [PubMed: 19118215]

Bartholin L, Cyprian FS, Vincent D, Garcia CN, Martel S, Horvat B, Berthet C, Goddard-Leon S, Treilleux I, Rimokh R, and Marie JC (2008). Generation of mice with conditionally activated transforming growth factor beta signaling through the TbetaRI/ALK5 receptor. Genesis 46, 724–731. [PubMed: 18821589]

Bedoui S, Whitney PG, Waithman J, Eidsmo L, Wakim L, Caminschi I, Allan RS, Wojtasiak M, Shortman K, Carbone FR, et al. (2009). Cross-presentation of viral and self antigens by skin-derived CD103+ dendritic cells. Nat Immunol 10, 488–495. [PubMed: 19349986]

Bobr A, Igyarto BZ, Haley KM, Li MO, Flavell RA, and Kaplan DH (2012). Autocrine/paracrine TGF-beta1 inhibits Langerhans cell migration. Proc Natl Acad Sci U S A 109, 10492–10497. [PubMed: 22689996]

Casey KA, Fraser KA, Schenkel JM, Moran A, Abt MC, Beura LK, Lucas PJ, Artis D, Wherry EJ, Hogquist K, et al. (2012). Antigen-independent differentiation and maintenance of effector-like resident memory T cells in tissues. J Immunol 188, 4866–4875. [PubMed: 22504644]

Chaudhri VK, Dienger-Stambaugh K, Wu Z, Shrestha M, and Singh H (2020). Charting the cis-regulome of activated B cells by coupling structural and functional genomics. Nat Immunol 21, 210–220. [PubMed: 31873292]

Collins N, Jiang X, Zaid A, Macleod BL, Li J, Park CO, Haque A, Bedoui S, Heath WR, Mueller SN, et al. (2016). Skin CD4(+) memory T cells exhibit combined cluster-mediated retention and equilibration with the circulation. Nat Commun 7, 11514. [PubMed: 27160938]

Falcon S, and Gentleman R (2007). Using GOstats to test gene lists for GO term association. Bioinformatics 23, 257–258. [PubMed: 17098774]

Gamradt P, Laoubi L, Nosbaum A, Mutez V, Lenief V, Grande S, Redoules D, Schmitt AM, Nicolas JF, and Vocanson M (2019). Inhibitory checkpoint receptors control CD8(+) resident memory T cells to prevent skin allergy. J Allergy Clin Immunol 143, 2147–2157 e2149. [PubMed: 30654051]

Gebhardt T, Whitney PG, Zaid A, Mackay LK, Brooks AG, Heath WR, Carbone FR, and Mueller SN (2011). Different patterns of peripheral migration by memory CD4+ and CD8+ T cells. Nature 477, 216–219. [PubMed: 21841802]

Henderson NC, Arnold TD, Katamura Y, Giacomini MM, Rodriguez JD, McCarty JH, Pellicoro A, Raschperger E, Betsholtz C, Ruminski PG, et al. (2013). Targeting of alphav integrin identifies a core molecular pathway that regulates fibrosis in several organs. Nat Med 19, 1617–1624. [PubMed: 24216753]

Hirai T, Whitley SK, and Kaplan DH (2020). Migration and Function of Memory CD8(+) T Cells in Skin. J Invest Dermatol 140, 748–755. [PubMed: 31812277]

Hirai T, Zenke Y, Yang Y, Bartholin L, Beura LK, Masopust D, and Kaplan DH (2019). Keratinocyte-Mediated Activation of the Cytokine TGF-beta Maintains Skin Recirculating Memory CD8(+) T Cells. Immunity 50, 1249–1261 e1245. [PubMed: 30952606]

Hobbs SJ, and Nolz JC (2019). Targeted Expansion of Tissue-Resident CD8(+) T Cells to Boost Cellular Immunity in the Skin. Cell Rep 29, 2990–2997 e2992. [PubMed: 31801067]

Jiang X, Clark RA, Liu L, Wagers AJ, Fuhlbrigge RC, and Kupper TS (2012). Skin infection generates non-migratory memory CD8+ T(RM) cells providing global skin immunity. Nature 483, 227–231. [PubMed: 22388819]

Khan TN, Mooster JL, Kilgore AM, Osborn JF, and Nolz JC (2016). Local antigen in nonlymphoid tissue promotes resident memory CD8+ T cell formation during viral infection. J Exp Med 213, 951–966. [PubMed: 27217536]

Kim D, Pertea G, Trapnell C, Pimentel H, Kelley R, and Salzberg SL (2013). TopHat2: accurate alignment of transcriptomes in the presence of insertions, deletions and gene fusions. Genome Biol 14, R36. [PubMed: 23618408]

Kish DD, Li X, and Fairchild RL (2009). CD8 T cells producing IL-17 and IFN-gamma initiate the innate immune response required for responses to antigen skin challenge. J Immunol 182, 5949–5959. [PubMed: 19414746]

Langmead B, and Salzberg SL (2012). Fast gapped-read alignment with Bowtie 2. Nat Methods 9, 357–359. [PubMed: 22388286]

Lee YT, Suarez-Ramirez JE, Wu T, Redman JM, Bouchard K, Hadley GA, and Cauley LS (2011). Environmental and antigen receptor-derived signals support sustained surveillance of the lungs by pathogen-specific cytotoxic T lymphocytes. J Virol 85, 4085–4094. [PubMed: 21345961]

Liu C, Somasundaram A, Manne S, Gocher AM, Szymczak-Workman AL, Vignali KM, Scott EN, Normolle DP, John Wherry E, Lipson EJ, et al. (2020). Neuropilin-1 is a T cell memory checkpoint limiting long-term antitumor immunity. Nat Immunol.

Liu L, Fuhlbrigge RC, Karibian K, Tian T, and Kupper TS (2006). Dynamic programming of CD8+ T cell trafficking after live viral immunization. Immunity 25, 511–520. [PubMed: 16973385]

Mackay LK, Rahimpour A, Ma JZ, Collins N, Stock AT, Hafon ML, Vega-Ramos J, Lauzurica P, Mueller SN, Stefanovic T, et al. (2013). The developmental pathway for CD103(+)CD8+ tissue-resident memory T cells of skin. Nat Immunol 14, 1294–1301. [PubMed: 24162776]

Mackay LK, Stock AT, Ma JZ, Jones CM, Kent SJ, Mueller SN, Heath WR, Carbone FR, and Gebhardt T (2012). Long-lived epithelial immunity by tissue-resident memory T (TRM) cells in the absence of persisting local antigen presentation. Proc Natl Acad Sci U S A 109, 7037–7042. [PubMed: 22509047]

Mackay LK, Wynne-Jones E, Freestone D, Pellicci DG, Mielke LA, Newman DM, Braun A, Masson F, Kallies A, Belz GT, and Carbone FR (2015). T-box Transcription Factors Combine with the Cytokines TGF-beta and IL-15 to Control Tissue-Resident Memory T Cell Fate. Immunity 43, 1101–1111. [PubMed: 26682984]

Mani V, Bromley SK, Aijo T, Mora-Buch R, Carrizosa E, Warner RD, Hamze M, Sen DR, Chasse AY, Lorant A, et al. (2019). Migratory DCs activate TGF-beta to precondition naive CD8(+) T cells for tissue-resident memory fate. Science 366.

Marie JC, Liggitt D, and Rudensky AY (2006). Cellular mechanisms of fatal early-onset autoimmunity in mice with the T cell-specific targeting of transforming growth factor-beta receptor. Immunity 25, 441–454. [PubMed: 16973387]

Masopust D, and Soerens AG (2019). Tissue-Resident T Cells and Other Resident Leukocytes. Annu Rev Immunol 37, 521–546. [PubMed: 30726153]

McMaster SR, Wein AN, Dunbar PR, Hayward SL, Cartwright EK, Denning TL, and Kohlmeier JE (2018). Pulmonary antigen encounter regulates the establishment of tissue-resident CD8 memory T cells in the lung airways and parenchyma. Mucosal Immunol 11, 1071–1078. [PubMed: 29453412]

Mohammed J, Beura LK, Bobr A, Astry B, Chicoine B, Kashem SW, Welty NE, Igyarto BZ, Wijeyesinghe S, Thompson EA, et al. (2016). Stromal cells control the epithelial residence of DCs and memory T cells by regulated activation of TGF-beta. Nat Immunol 17, 414–421. [PubMed: 26901152]

Muschaweckh A, Buchholz VR, Fellenzer A, Hessel C, Konig PA, Tao S, Tao R, Heikenwalder M, Busch DH, Korn T, et al. (2016). Antigen-dependent competition shapes the local repertoire of tissue-resident memory CD8+ T cells. J Exp Med 213, 3075–3086. [PubMed: 27899444]

Pan Y, Tian T, Park CO, Lofftus SY, Mei S, Liu X, Luo C, O'Malley JT, Gehad A, Teague JE, et al. (2017). Survival of tissue-resident memory T cells requires exogenous lipid uptake and metabolism. Nature 543, 252–256. [PubMed: 28219080]

Park SL, Zaid A, Hor JL, Christo SN, Prier JE, Davies B, Alexandre YO, Gregory JL, Russell TA, Gebhardt T, et al. (2018). Local proliferation maintains a stable pool of tissue-resident memory T cells after antiviral recall responses. Nat Immunol 19, 183–191. [PubMed: 29311695]

Qin Y, Garrison BS, Ma W, Wang R, Jiang A, Li J, Mistry M, Bronson RT, Santoro D, Franco C, et al. (2018). A Milieu Molecule for TGF-beta Required for Microglia Function in the Nervous System. Cell 174, 156–171 e116. [PubMed: 29909984]

Reynoso GV, Weisberg AS, Shannon JP, McManus DT, Shores L, Americo JL, Stan RV, Yewdell JW, and Hickman HD (2019). Lymph node conduits transport virions for rapid T cell activation. Nat Immunol 20, 602–612. [PubMed: 30886418]

Richmond JM, Strassner JP, Zapata L Jr., Garg M, Riding RL, Refat MA, Fan X, Azzolino V, Tovar-Garza A, Tsurushita N, et al. (2018). Antibody blockade of IL-15 signaling has the potential to durably reverse vitiligo. Sci Transl Med 10.

Sheridan BS, Pham QM, Lee YT, Cauley LS, Puddington L, and Lefrancois L (2014). Oral infection drives a distinct population of intestinal resident memory CD8(+) T cells with enhanced protective function. Immunity 40, 747–757. [PubMed: 24792910]

Slutter B, Van Braeckel-Budimir N, Abboud G, Varga SM, Salek-Ardakani S, and Harty JT (2017). Dynamics of influenza-induced lung-resident memory T cells underlie waning heterosubtypic immunity. Sci Immunol 2.

Steinert EM, Schenkel JM, Fraser KA, Beura LK, Manlove LS, Igyarto BZ, Southern PJ, and Masopust D (2015). Quantifying Memory CD8 T Cells Reveals Regionalization of Immunosurveillance. Cell 161, 737–749. [PubMed: 25957682]

Tran DQ, Andersson J, Wang R, Ramsey H, Unutmaz D, and Shevach EM (2009). GARP (LRRC32) is essential for the surface expression of latent TGF-beta on platelets and activated FOXP3+ regulatory T cells. Proc Natl Acad Sci U S A 106, 13445–13450. [PubMed: 19651619]

Trapnell C, Williams BA, Pertea G, Mortazavi A, Kwan G, van Baren MJ, Salzberg SL, Wold BJ, and Pachter L (2010). Transcript assembly and quantification by RNA-Seq reveals unannotated transcripts and isoform switching during cell differentiation. Nat Biotechnol 28, 511–515. [PubMed: 20436464]

Vezys V, Yates A, Casey KA, Lanier G, Ahmed R, Antia R, and Masopust D (2009). Memory CD8 T-cell compartment grows in size with immunological experience. Nature 457, 196–199. [PubMed: 19005468]

Vincent DF, Kaniewski B, Powers SE, Havenar-Daughton C, Marie JC, Wotton D, and Bartholin L (2010). A rapid strategy to detect the recombined allele in LSL-TbetaRICA transgenic mice. Genesis 48, 559–562. [PubMed: 20645310]

Wakim LM, Smith J, Caminschi I, Lahoud MH, and Villadangos JA (2015). Antibody-targeted vaccination to lung dendritic cells generates tissue-resident memory CD8 T cells that are highly protective against influenza virus infection. Mucosal Immunol 8, 1060–1071. [PubMed: 25586557]

Worthington JJ, Klementowicz JE, and Travis MA (2011). TGFbeta: a sleeping giant awoken by integrins. Trends Biochem Sci 36, 47–54. [PubMed: 20870411]

Yang Y, Zenke Y, Hirai T, and Kaplan DH (2019). Keratinocyte-derived TGFbeta is not required to maintain skin immune homeostasis. J Dermatol Sci 94, 290–297. [PubMed: 31118160]

Yang Z, Mu Z, Dabovic B, Jurukovski V, Yu D, Sung J, Xiong X, and Munger JS (2007). Absence of integrin-mediated TGFbeta1 activation in vivo recapitulates the phenotype of TGFbeta1-null mice. J Cell Biol 176, 787–793. [PubMed: 17353357]

Zaid A, Mackay LK, Rahimpour A, Braun A, Veldhoen M, Carbone FR, Manton JH, Heath WR, and Mueller SN (2014). Persistence of skin-resident memory T cells within an epidermal niche. Proc Natl Acad Sci U S A 111, 5307–5312. [PubMed: 24706879]

Key Points

1. Long-term persistence of epidermal Trm cells requires transactivated autocrine TGFβ
2. Epidermal bystander Trm cells are depleted when active TGFβ is limited
3. Competition for TGFβ allows newly recruited effectors to replace bystander Trm cells
4. Intraclonal competition for active TGFβ shapes Trm occupancy in the epidermal niche

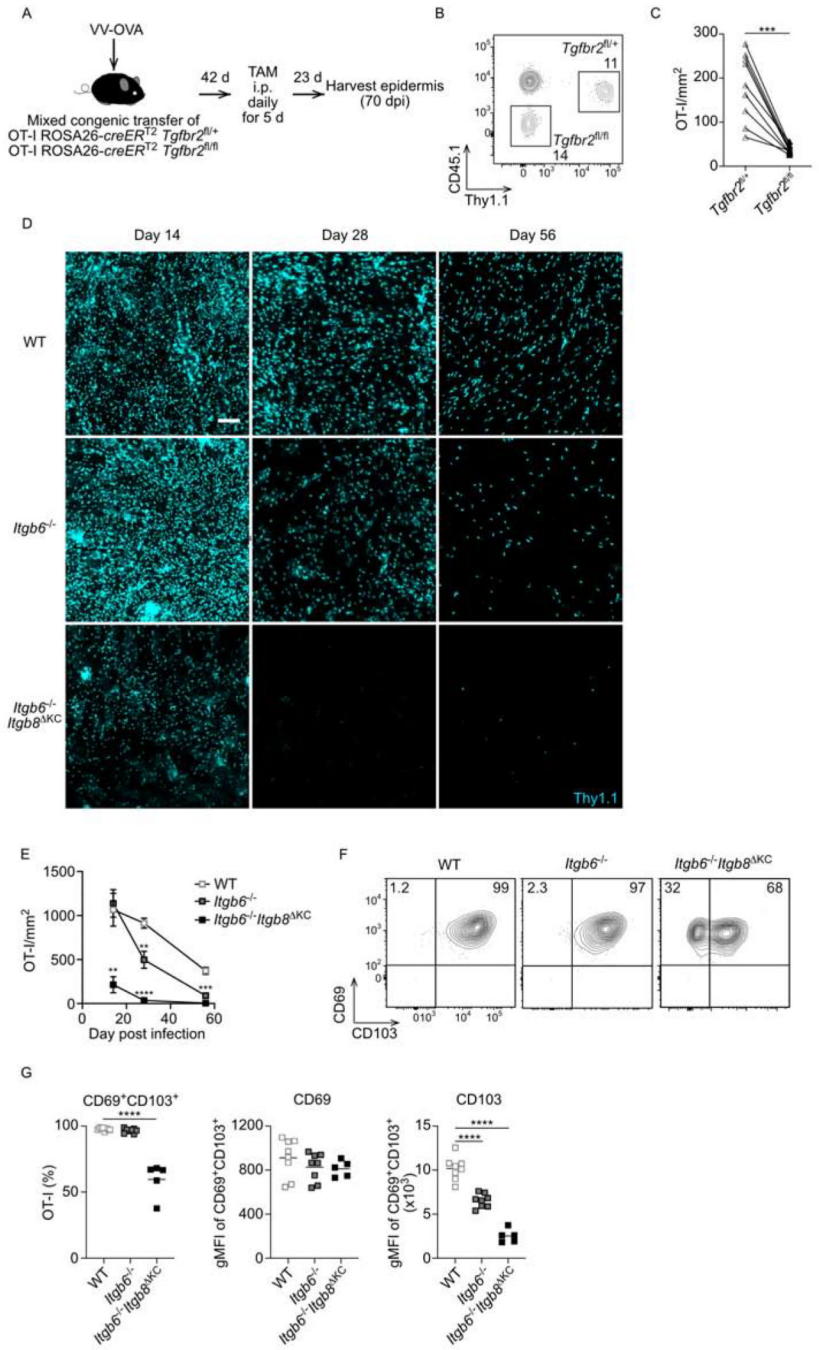

Figure 1. Trm cells require TGFβ signaling and transactivated TGFβ for epidermal persistence

(A) Experimental scheme for testing a TGFβ signaling requirement for Trm cell persistence. Naïve CD8$^+$ T cells from OT-I ROSA26-*cre*ER^{T2} x *Tgfbr2*$^{f/+}$ (Thy 1.1/Thy1.2, CD45.1/CD45.2) and OT-I ROSA26-*cre*ER^{T2} x *Tgfbr2*$^{fl/fl}$ (Thy1.2/Thy1.2, CD45.2/CD45.2) mice were adoptively transferred into CD45.1/CD45.1 recipient mice followed by skin VV-OVA infection. (B) Representative flow plot of peripheral blood at day 7 post infection. gated on live CD3$^+$CD8α$^+$ T cells is shown. (C) Quantification of OT-I cells in epidermal whole mount 23 days post tamoxifen are shown. (D) Thy1.1$^+$ OT-I mice were transferred to WT,

Itgb6$^{-/-}$, or *Itgb6*$^{-/-}$*Itgb8*$^{\Delta KC}$ mice followed by VV-OVA skin infection. Representative immunofluorescence images of epidermal whole mount stained for Thy1.1^{+} OT-I cells are shown. (E) Summary data at the indicated time points from (D) is shown. (F) Representative flow plots and (G) summary data of epidermal cells gated on live CD45^{+}Thy1.1^{+} OT-I cells are shown. Data are representative of two (B-C) or three separate experiments (D-G). Each symbol represents data from an individual animal (C, G) or pooled data with at least three mice per point (E) and lines indicate data from the same animal. Data are mean ± SEM. **p < 0.01, ***p < 0.001, and ****p < 0.0001. Scale bar represents 100 μm. TAM, tamoxifen; dpi, days post-infection; gMFI, geometric mean fluorescence intensity. See also Figure S1.

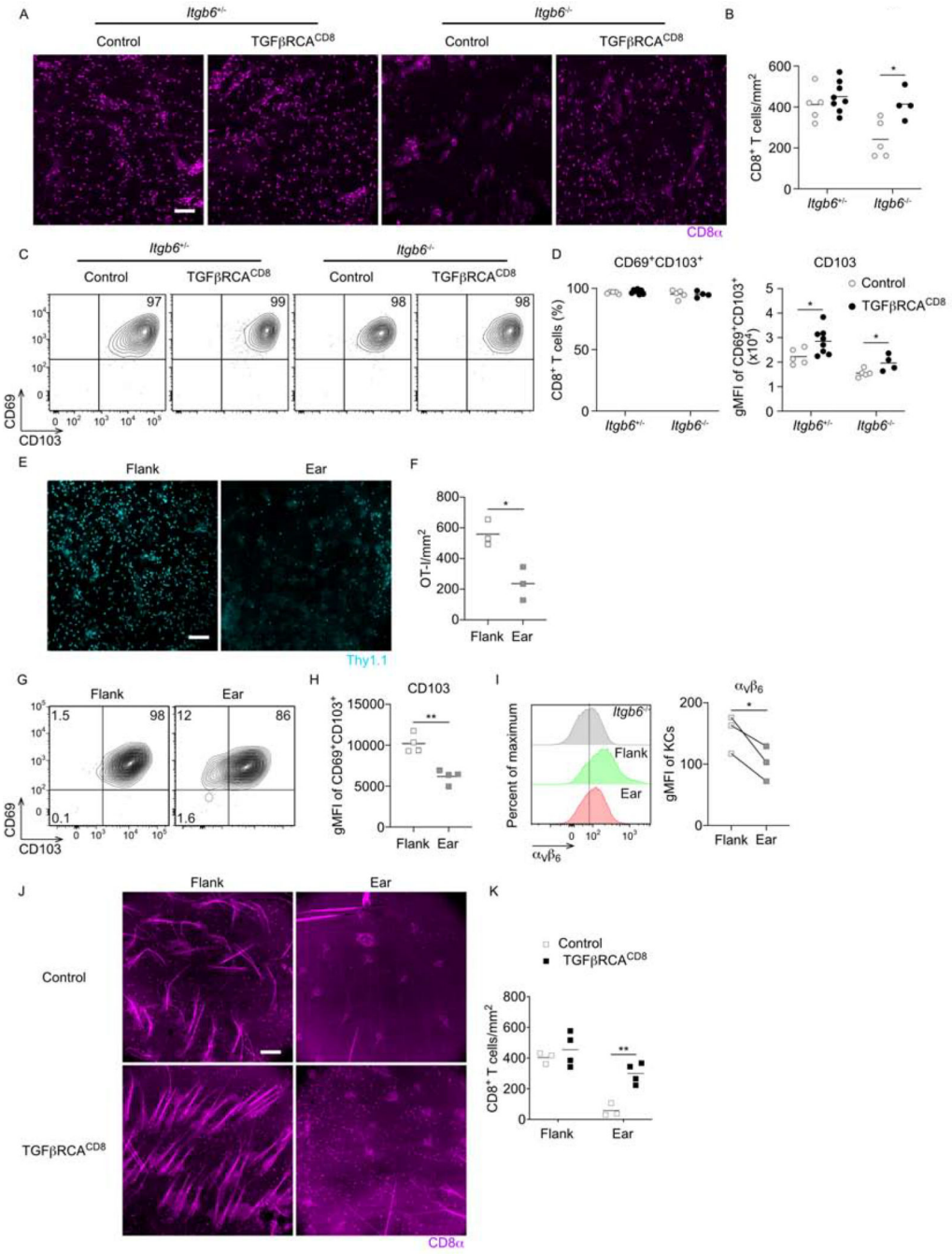

Figure 2. TGFβR signaling rescues Trm cell numbers in absence of $\alpha_v\beta_6$

(A-D) TGFβRCA^{CD8} x *Itgb6*$^{-/+}$, TGFβRCA^{CD8} x *Itgb6*$^{-/-}$, and control *Itgb6*$^{-/+}$ and *Itgb6*$^{-/-}$ mice were infected with VV-OVA on flank skin and treated with tamoxifen i.p. on days 7–11 post infection. (A) Representative immunofluorescence images and (B) summary data of epidermal whole mount for stained for CD8α$^+$ harvested on day 46 post infection are shown. (C) Representative flow plots gated on live CD45$^+$TCRβ$^+$CD8α$^+$ CD8$^+$ T cells in epidermis and (D) the percentage of CD8$^+$ T cells expressing CD69 and CD103 as well as CD103 gMFI of CD69$^+$CD103$^+$ CD8$^+$ T cells. (E) WT OT-I transferred mice were dual

infected on ear and flank with VV-OVA. Representative immunofluorescence images and (F) summary data of epidermal whole mounts stained for Thy1.1^{+} OT-I cells are shown. (G) Representative flow plots gated on live CD45^{+}Thy1.1^{+} OT-I cells in epidermis and (H) gMFI of CD103^{+} on OT-I cells is shown. (I) Representative flow plot of KCs from naive *Itgb6*$^{-/-}$ flank (gray), WT flank (green), and WT ear (red) gated on live CD45^{-} cells and gMFI of $\alpha_v\beta_6$ are shown. (J) TGFβRCA^{CD8} and control mice were dual infected on flank and ear with VV-OVA followed by tamoxifen i.p. on day 14-dpi. Representative immunofluorescence images of flank or ear epidermal whole mount for CD8α^{+} CD8^{+} T cells and (K) summary data are shown. Data are representative of two (E-I) or three (A-D) separate experiments. Each symbol represents data from an individual animal. **$p < 0.01$, ***$p < 0.001$, and ****$p < 0.0001$. Scale bar represents 100 μm. gMFI, geometric mean fluorescence intensity. See also Figure S2.

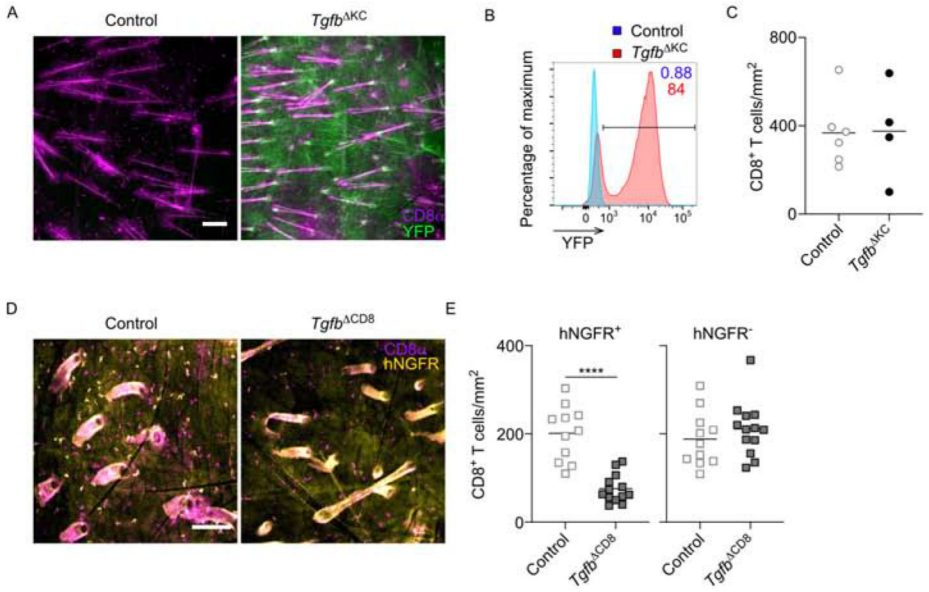

Figure 3. Epidermal Trm cells require autocrine TGFβ

(A) Control (*Tgfb1*$^{fl/fl}$) and *Tgfb*$^{\Delta KC}$ (*Krt14-cre*ER^{T2} x *Tgfb1*$^{fl/fl}$) mice with a YFP reporter were skin infected with VV followed by topical treatment of 4-OH tamoxifen for two consecutive days starting at least on day 42 post infection. Representative immunofluorescence images of epidermal whole mounts harvested on day 21 after the last tamoxifen treatment stained for CD8α^{+} (magenta) and YFP (green). (B) Representative flow plot gated on live CD45^{-} KCs is shown. (C) Summary data from (A) is shown. (D) Control (E8I-*cre*ER^{T2} x *Tgfb1*$^{fl/+}$) and *Tgfb*$^{\Delta CD8}$ (E8I-*cre*ER^{T2} x *Tgfb1*$^{fl/fl}$) mice with a human nerve growth factor receptor reporter (hNGFR) were infected with VV followed by i.p. tamoxifen starting at least day 42 post infection. Representative epidermal whole mounts harvested 21 days after the last tamoxifen treatment and stained for CD8α^{+} (magenta) and hNGFR (yellow) are shown. (E) Summary data from (D). Data are representative of two (D and E) or three (A-C) separate experiments. ****p < 0.0001. Scale bar represents 100 μm.

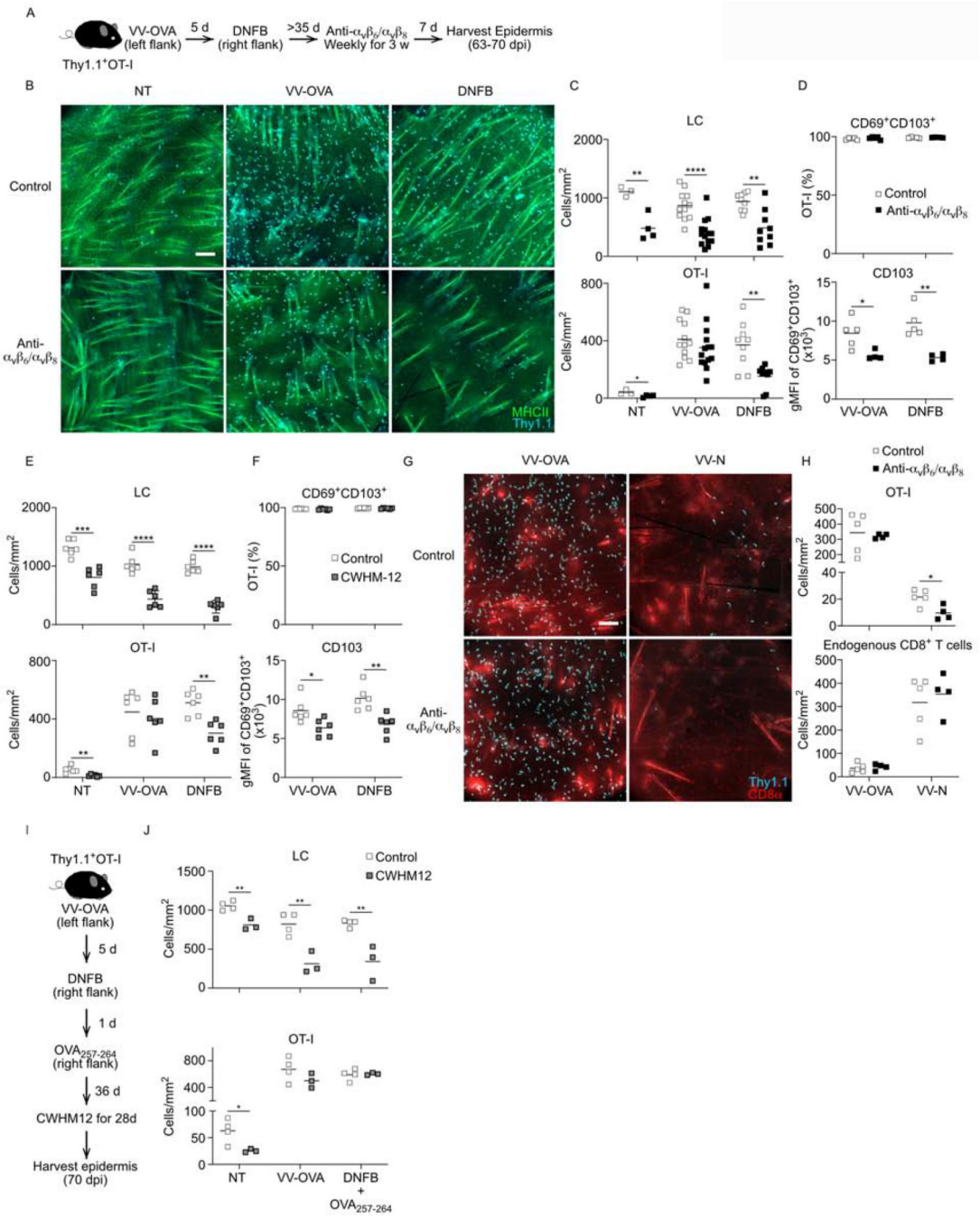

Figure 4. Blockade of integrin-mediated TGFβ activation reduces bystander Trm cells

(A) Experimental scheme. Thy1.1$^+$ OT-I cells were adoptively transferred into naïve WT mice followed by skin VV-OVA infection on left flank. On day 5 post infection, the right flank was painted with 0.15% DNFB. The mice were injected weekly with anti-$\alpha_v\beta_6$ and $\alpha_v\beta_8$ mAbs starting on day 42–49 post infection for a total of 3 weeks. The epidermis from 'not treated' abdomen (NT), left flank (VV-OVA), and right flank (DNFB-pulled) were harvested 7 days after the last mAbs treatment. (B) Representative immunofluorescence images of epidermal whole mounts stained for MHCII$^+$ (green, LC) and Thy1.1$^+$ (cyan, OT-

I) cells are shown. (C) Quantification of LC and OT-I numbers from control (open squares) and mAb treat mice (closed squares) are shown. (D) Frequency of $CD69^+CD103^+$ OT-I cells gated on live $CD45^+Thy1.1^+$ cells and CD103 gMFI of $CD69^+CD103^+$ OT-I cells are shown. (E) Mice were treated as in A, except CWHM-12 or control was delivered by implantable ALZET osmotic minipumps for 28 days instead of mAbs. Quantification of LC and OT-I cells from epidermal whole mounts are shown. (F) Frequency of $CD69^+CD103^+$ OT-I cells gated on live $CD45^+Thy1.1^+$ cells and CD103 gMFI of $CD69^+CD103^+$ OT-I cells are shown. (G) OT-I adoptive transfer mice were dual infected with VV-OVA and VV-N on opposite flanks and treated with anti-$\alpha_v\beta_6$ and $\alpha_v\beta_8$ mAbs for 3 weeks starting on day 49 post infection. Representative epidermal whole mounts from VV-OVA and VV-N sites harvested 7 days after the last mAb or control treatment are shown. (H) Quantification of the number of $Thy1.1^+$ $CD8^+$ OT-I and endogenous Thy 1.1^- $CD8^+$ T cells is shown. (I) Experimental scheme. As in (A) except that $OVA_{257–264}$ peptide was applied to the DNFB-pulled sites 1 day after DNFB painting and treated with CWHM-12 instead of the mAbs. (J) Quantification of the number of $MHC\text{-}II^+$ LC and $Thy1.1^+$ OT-I cells in epidermal whole mounts is shown. Data are representative of two (E-J) or three (A-D) separate experiments. Each symbol represents data from an individual animal. *$p < 0.05$, **$p < 0.01$, and ****$p < 0.0001$. Scale bar represents 100 μm. gMFI, geometric mean fluorescence intensity. See also Figure S3.

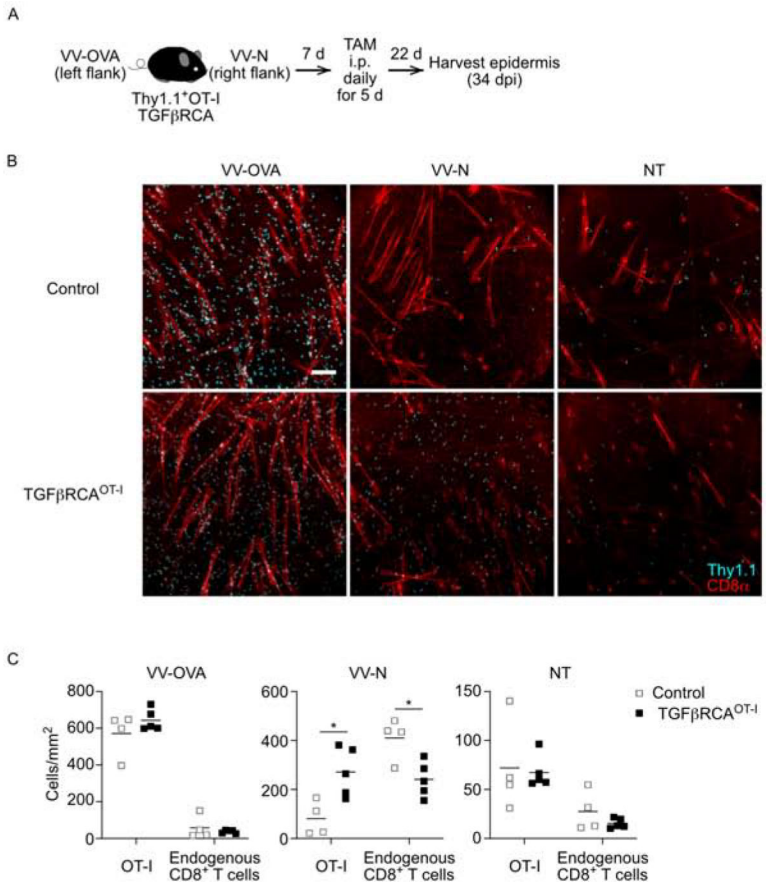

Figure 5. TGFβ signaling provides a competitive advantage during Trm cell development

(A) Experimental scheme. Thy1.1$^+$ OT-I or OT-I TGFβRICA were transferred to WT mice followed by dual infection of VV-OVA and VV-N on opposite flanks. Mice were treated with tamoxifen i.p. for 5 consecutive days starting on day 7. Representative immunofluorescence images of epidermal whole mounts stained for Thy1.1 (cyan, OT-I cells) and CD8α (red) from left flank (VV-OVA), right flank (VV-N), and not treated abdomen (NT) sites harvested day 34 post infection are shown. (C) Summary data showing numbers of OT-I (Thy1.1$^+$CD8α$^+$) and endogenous CD8$^+$ T cells (Thy1.1$^-$CD8α$^+$) from OT-I TGFβRICA (closed squares) and control OT-I (open squares) recipients are shown. Each symbol represents data from an individual animal (C). Data are representative of three separate experiments. *$p < 0.05$. Scale bar represents 100 μm.

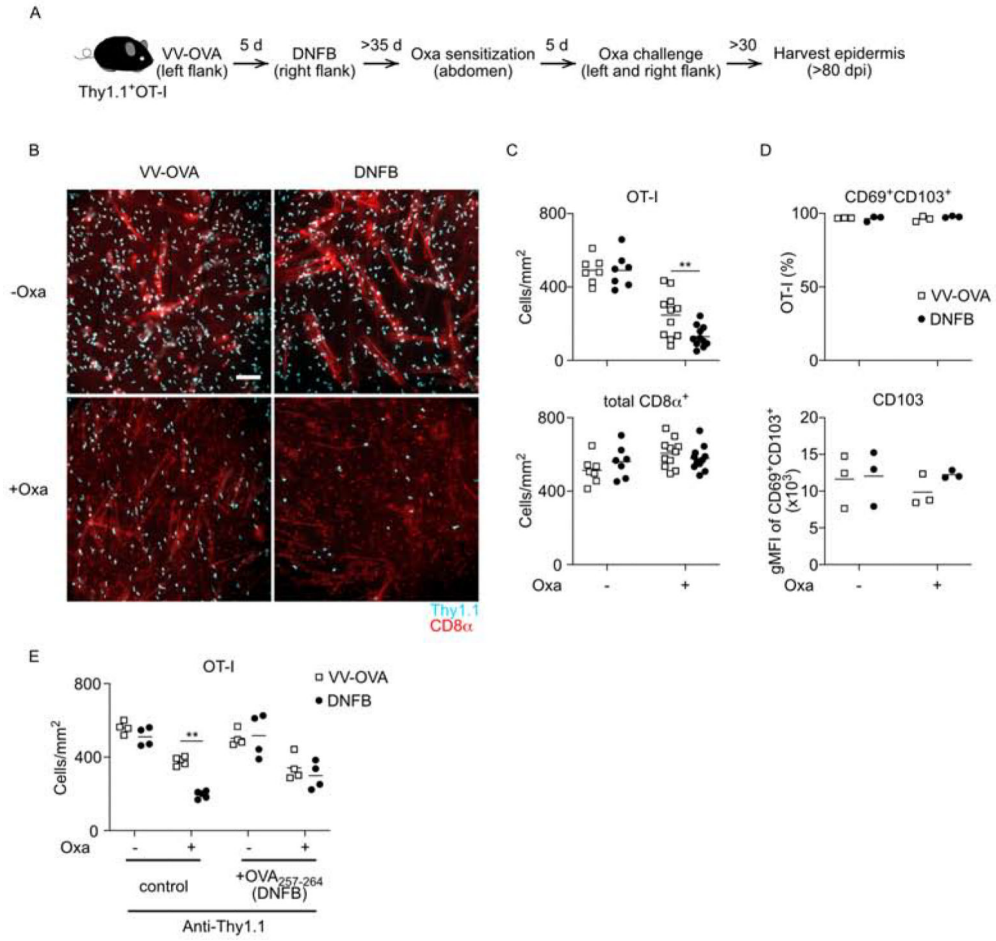

Figure 6. Bystander Trm cells are preferentially displaced by newly recruited CD8$^+$ T cells

(A) Experimental scheme. Thy1.1$^+$ OT-I cells were adoptively transferred into naïve WT mice followed by skin VV-OVA infection on left flank. On day 5 post infection, the right flank was painted with 0.15% DNFB. More than 35 days after DNFB treatment, mice were sensitized at abdomen with oxazolone and 5 days later both flanks were challenged by oxazolone. (B) Representative immunofluorescence images of epidermal whole mounts harvested at least 30 days post oxazolone challenge stained for Thy1.1$^+$ (cyan) and CD8α$^+$ (red) are shown. (C) Summary data showing numbers of OT-I (Thy1.1+, CD8α$^+$) and total CD8$^+$ T cells (Thy1.1$^{-/+}$CD8α$^+$). (D) The frequency of CD69$^+$CD103$^+$ OT-I cells gated on live CD45$^+$Thy1.1$^+$ and CD103 gMFI of CD69$^+$CD103$^+$ OT-I cells from VV-OVA sites (open squares) and DNFB-pulled sites (closed circles) are shown. (E) WT mice were treated as in (A), but all mice were treated i.p. with titrated anti-Thy1.1 depleting antibody before oxazolone challenge and some groups were treated with epicutaneous $OVA_{257–264}$ peptide on DNFB-treated flank day 6 post infection. Quantification of OT-I from epidermal whole mounts is shown. Each symbol represents data from an individual animal. Data are representative of two (E) or three (B-D) separate experiments. **p < 0.01. Scale bar represents 100 μm. Oxa, oxazolone; gMFI, geometric mean fluorescence intensity. See also Figure S4.

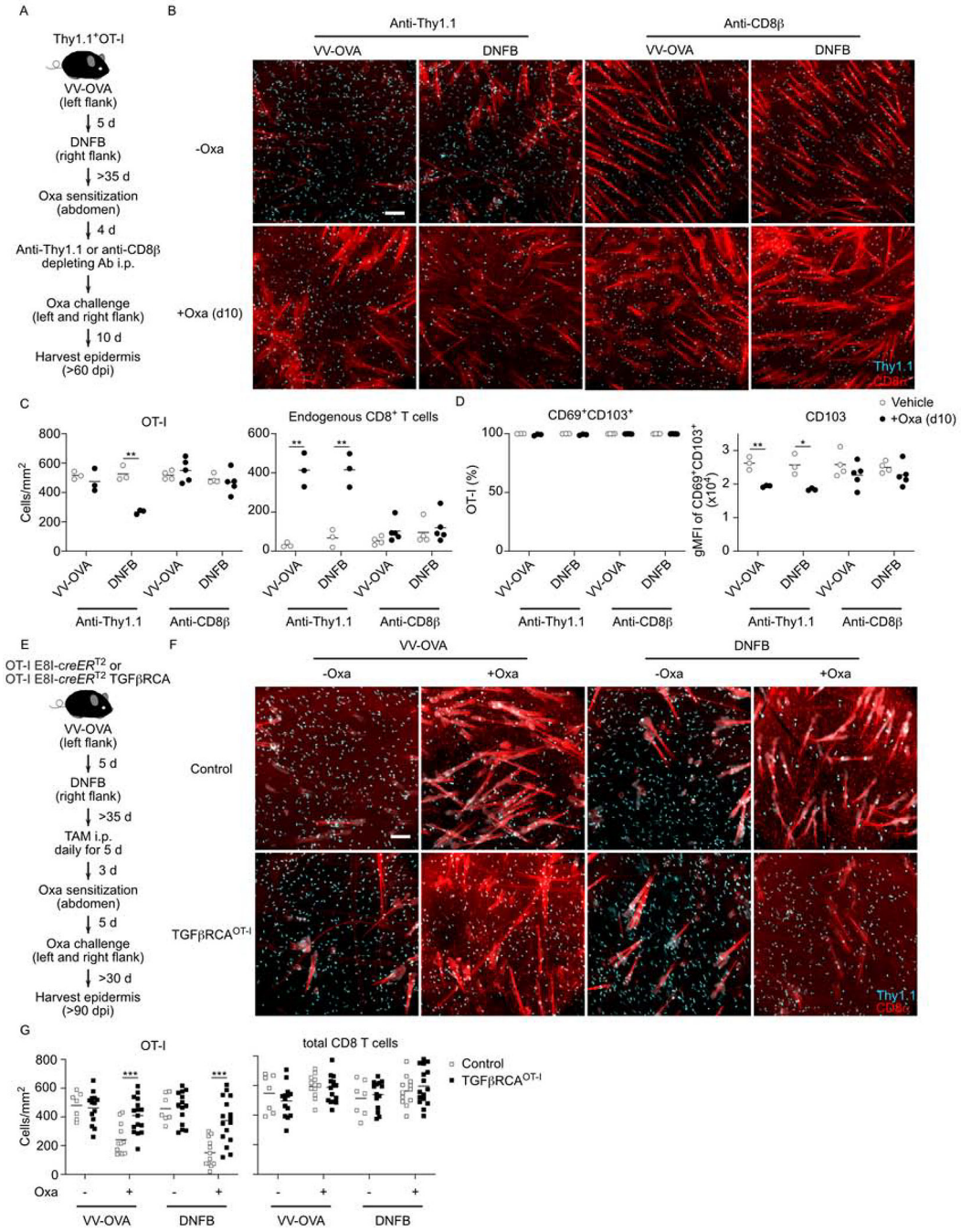

Figure 7. Competition for active TGFβ allows for preferential retention of antigen-specific Trm cells

(A) Experimental scheme. Cohorts of mice were treated as in Figure 6A except titrated anti-Thy1.1 or anti-CD8β depleting antibodies were administered prior to oxazolone challenge. (B) Representative immunofluorescence images of epidermal whole mounts harvested at 10 days post oxazolone challenge stained for Thy1.1$^+$ (cyan) and CD8α$^+$ (red) are shown. (C) Summary data showing numbers of OT-I (Thy1.1$^+$CD8α$^+$) and endogenous CD8$^+$ T cells (Thy1.1$^-$CD8α$^+$) from mice challenged with oxazolone (closed circles) or vehicle (open circles). (D) The frequency of CD69$^+$CD103$^+$ OT-I cells gated on live CD45$^+$Thy1.1$^+$ and

gMFI CD103$^+$ from VV-OVA are shown. (E) Experimental scheme. As in (A) except that WT mice were adoptively transferred with control OT-I (E8I-*cre*ER^{T2}) or OT-I TGFβRCA (E8I-*cre*ER^{T2} x TGFβRCA). Prior to oxazolone sensitization, mice were treated i.p. tamoxifen for 5 consecutive days. (F) Representative immunofluorescence images of epidermal whole mounts harvested at least 34 days post oxazolone challenge stained for Thy1.1$^+$ (cyan) and CD8α$^+$ (red) are shown. (G) Summary data showing numbers of OT-I (Thy1.1$^+$CD8α$^+$) and total CD8$^+$ T cells (Thy1.1$^{+/-}$CD8α$^+$) from mice transferred with control OT-I (open squares) or OT-I TGFβRCA (closed squares) is shown. Data are representative of two (B-D) or three (F and G) separate experiments. *$p < 0.05$, **$p < 0.01$, and ***$p < 0.001$. Scale bar represents 100 μm. Oxa, oxazolone; gMFI, geometric mean fluorescence intensity. See also Figure S4, S5, and Table S1.

KEY RESOURCES TABLE

REAGENT or RESOURCE	SOURCE	IDENTIFIER
Antibodies		
Brilliant Violet 605 anti-mouse CD8a (53–6.7)	BioLegend	Cat# 100744, RRID:AB_2562609
Alexa Fluor 488 anti-mouse CD8a (53–6.7)	BioLegend	Cat# 100723, RRID:AB_ 389304
Alexa Fluor 594 anti-mouse CD8a (53–6.7)	BioLegend	Cat# 100758, RRID:AB_2563237
Alexa Fluor 647 anti-mouse CD8a (53–6.7)	BioLegend	Cat# 100724, RRID:AB_2722580
BUV737 anti-mouse CD8a (53–6.7)	BD Biosciences	Cat# 564297, RRID:AB_2563103
anti-mouse CD8b (H35–17.2)	Thermo Fisher Scientific	Cat# 14–0083-82, RRID:AB_657757
Alexa Fluor 700 anti-mouse CD3 (17A2)	BioLegend	Cat# 100216, RRID:AB_493697
PerCP/Cyanine5.5 anti-mouse CD3 (17A2)	BioLegend	Cat# 100218, RRID:AB_1595492
Brilliant Violet 510 anti-mouse/human CD44 (IM7)	BD Biosciences	Cat# 563114, RRID:AB_2738011
PerCP/Cyanine5.5 anti-mouse/human CD44 (IM7)	BioLegend	Cat# 103032, RRID:AB_2076204
PE/Dazzle 594 anti-mouse TCR β chain (H57–597)	BioLegend	Cat# 109240, RRID:AB_2565655
Alexa Fluor 700 anti-mouse CD90.2 (30-H12)	BioLengend	Cat# 105320, RRID:AB_493725
Alexa Fluor 647 anti-mouse CD90.1 (OX-7)	BioLengend	Cat# 202508, RRID:AB_492884
BUV 395 anti-mouse CD90.1 (OX-7)	BD Biosciences	Cat# 740261, RRID:AB_2721773
anti-mouse CD90.1 (HIS51)	Thermo Fisher Scientific	Cat# 14–0900-81, RRID:AB_467373
BUV737 anti-mouse CD69 (H1.2F3)	BD Biosciences	Cat# 564684, RRID:AB_2738891
PE/Cy7 anti-mouse CD69 (H1.2F3)	BioLegend	Cat# 104512, RRID:AB_493564
Brilliant Violet 510 anti-mouse CD103 (2E7)	BioLegend	Cat# 121423, RRID:AB_2562713
Alexa Fluor 647 anti-mouse CD103 (2E7)	BioLegend	Cat# 121410, RRID:AB_535952
PerCP/Cyanine5.5 anti-mouse CD45.2 (104)	BioLegend	Cat# 109828, RRID:AB_893350
Alexa Fluor 488 anti-mouse CD45.2 (104)	BioLegend	Cat# 109816, RRID:AB_492868
APC anti-mouse CD45.2 (104)	BioLegend	Cat# 109814, RRID:AB_389211
Brilliant Violet 605 anti-mouse CD45.2 (104)	BioLegend	Cat# 109841, RRID:AB_2563485
PerCP/Cyanine5.5 anti-mouse CD45.1 (A20)	BioLegend	Cat# 110728, RRID:AB_893346
Brilliant Violet 605 anti-mouse IFN gamma (XMG1.2)	BioLegend	Cat# 505840, RRID:AB_2734493
PE anti-mouse IL-2 (JES6–5H4)	BioLegend	Cat# 503808, RRID:AB_315302
Brilliant Violet 421 anti-mouse TNF-α (MP6-XT22)	BioLegend	Cat# 506328, RRID:AB_2562902
Alexa Fluor 488 anti-mouse I-A/I-E (M5/114.15.2)	BioLegend	Cat# 107616, RRID:AB_493523
Alexa Fluor 647 anti-human CD271 (NGFR) (ME20.4)	BioLegend	Cat# 345114, RRID:AB_2572059
PE anti-human CD271 (NGFR) (ME20.4)	BioLegend	Cat# 345106, RRID:AB_2152647
Alexa Fluor 488 anti-GFP (FM264G)	BioLegend	Cat# 338008, RRID:AB_2563288
PE/Dazzle 594 anti-human GranzymeB (GB11)	BioLegend	Cat# 562462, RRID:AB_2737618
Phycoerythrin Polyclonal Antibody	Thermo Fisher Scientific	Cat# PA5–35006, RRID:AB_ 2552333
Anti-avb6 (6.3G9)	Dr. D. Sheppard, University of California	N/A
Anti-avb8 (ADWA-11)	Dr. D. Sheppard, University of California	N/A

REAGENT or RESOURCE	SOURCE	IDENTIFIER
Bacterial and Virus Strains		
Vaccinia virus- Western Reserve strain expressing $OVA_{257–264}$ (VV-OVA)	Dr. J. Yewdell, National Institute of Allergy and Infectious Diseases	N/A
Vaccinia virus- Western Reserve strain expressing nucleocapsid protein of vesicular stomatitis virus (VV-N)	Dr. J. Yewdell, National Institute of Allergy and Infectious Diseases	N/A
Chemicals, Peptides, and Recombinant Proteins		
$OVA_{257–264}$ (SIINFEKL)	ANASPEC	Cat# AS-62572–5
CWHM-12	Indalo therapeutics	N/A
Brefeldin A	Sigma-Aldrich	Cat# B6542
4-Ethoxymethylene-2-phenyl-2-oxazolin-5-one	Sigma-Aldrich	Cat# 862207
Deoxyribonuclease I	Sigma-Aldrich	Cat# D5025
Dimethyl sulfoxide	Sigma-Aldrich	Cat# D2650
Fetal Bovine Serum, Heat Inactivated	HyClone	Cat# 89133–096
2-Mercaptoethanol	Sigma-Aldrich	Cat# M6250
Penicillin-Streptomycin	Gibco	Cat# 15140122
MEM Nonessential Amino Acids	Corning	Cat# 25025CI
Sodium Azide, 5% (w/v) Aqueous Solution	Ricca Chemical	Cat# 71448–16
0.5M EDTA, pH 8.0	Invitrogen	Cat# 15–575–020
32% paraformaldehyde	Thermo Fisher Scientific	Cat# 50–980–495
Protein Transport Inhibitor Cocktail	eBioscience	Cat# 00–4980–03
Fixable Viability Dye eFluor™ 780	eBioscience	Cat# 65–0865–14
RPMI1640	Corning	Cat# 10040CV
Red Blood Cell Lysing Buffer Hybri-Max	Sigma Aldrich	Cat# R7757
Heparin sodium salt from porcine intestinal mucosa	Sigma Aldrich	Cat# H3393
HEPES solution	Sigma Aldrich	Cat# H0887
Corn oil	Sigma Aldrich	Cat# C8267
Tamoxifen	Sigma Aldrich	Cat# T5648
4-OH Tamoxifen	Sigma Aldrich	Cat# H7904–5MG
Critical Commercial Assays		
MojoSort™ Mouse CD8 T Cell Isolation Kit	BioLegend	Cat# 480035
TaqMan™ Gene Expression Master Mix	Applied Biosystems	Cat# 4369016
RNeasy Mini Kit	QIAGEN	Cat# 74104
High-Capacity cDNA Reverse Transcription Kit	Applied Biosystems	Cat# 4368814
Alexa Fluor™ 555 Antibody Labeling Kit	Thermo Fisher Scientific	Cat# A20187
TaqMan Gene Expression Assay Gapdh	Thermo Fisher Scientific	Cat# Mm99999915_g1
TaqMan Gene Expression Assay Itgb6	Thermo Fisher Scientific	Cat# Mm01269869_m1
TaqMan Gene Expression Assay Il7	Thermo Fisher Scientific	Cat# Mm01295803_m1
TaqMan Gene Expression Assay Il15	Thermo Fisher Scientific	Cat# Mm00434210_m1
Experimental Models: Organisms/Strains		

REAGENT or RESOURCE	SOURCE	IDENTIFIER
Mouse: WT: C57BL/6J	The Jackson Laboratory	Cat# JAX:000664, RRID:IMSR_JAX:000664
Mouse: K14-Cre: Tg(KRT14-cre)1Amc/J	The Jackson Laboratory	Cat# JAX:004782, RRID:IMSR_JAX:004782
Mouse: K14-CreERT : Tg(KRT14-cre/ERT)20Efu/J	The Jackson Laboratory	Cat# JAX: 005107, RRID:IMSR_JAX: 005107
Mouse: ROSA26.LSL.YFP: B6.129X1-Gt(ROSA)26Sortm1(EYFP)Cos/J	The Jackson Laboratory	Cat# JAX: 006148, RRID:IMSR_JAX: 006148
Mouse: OT-I: C57BL/6-Tg(TcraTcrb)1100Mjb/J	The Jackson Laboratory	Cat# JAX:003831, RRID:IMSR_JAX:003831
Mouse: $Rag^{-/-}$: B6.129S7-Rag1tm1Mom/J	The Jackson Laboratory	Cat# JAX:002216, RRID:IMSR_JAX:002216
Mouse: Thy1.1: CBy.PL(B6)-Thy1^{a}/ScrJ	The Jackson Laboratory	Cat# JAX:005443, RRID:IMSR_JAX:005443
Mouse: CD45.1: B6.SJL-Ptprca Pepcb/BoyJ	The Jackson Laboratory	Cat# JAX: 002014, RRID:IMSR_JAX:002014
Mouse: CD45.1: B6.SJL-Ptprca Pepcb/BoyJ	The Jackson Laboratory	Cat# JAX: 002014, RRID:IMSR_JAX:002014
Mouse: CD45.1: B6.SJL-Ptprca Pepcb/BoyJ	The Jackson Laboratory	Cat# JAX: 002014, RRID:IMSR_JAX:002014
Mouse: OT-I $CreER^{T2}$ TGFbRIIfl/fl	Dr. Thorsten Mempel Harvard University	N/A
Mouse: *Itgb6*$^{-/-}$	Dr. D. Sheppard, University of California	N/A
Mouse: *Itgb8*^{loxP}	Dr. D. Sheppard, University of California	N/A
Mouse: TGFβRI-CA	Dr. L. Bartholin, Centre de Recherche en Cancérologie de LYON	N/A
Mouse: E8ICreER^{T2}	Dr. D.A. Vignali, University of Pittsburgh	N/A
Mouse: ROSA26.LSL.hNGFR	Dr. D.A. Vignali, University of Pittsburgh	N/A
Oligonucleotides		
Software and Algorithms		
Prism 8	Graphpad Inc	RRID:SCR_002798
Flowjo v10	Treestar Inc	RRID:SCR_008520
ImageJ 64		RRID: SCR_003070
Paired RNAseq Data of Trm from VV-ova and DNFB sites	NCBI GEO	GSE156668

Author Manuscript

Author Manuscript

Author Manuscript

REAGENT or RESOURCE	SOURCE	IDENTIFIER